Master's Thesis

Multi-color Upconversion Luminescence Tuning by Thermal Process with Silica Nanoparticles

Subeen Shin

Department of Chemical Engineering

Graduate School of UNIST

2018

Multi-color Upconversion Luminescence Tuning by Thermal Process with Silica Nanoparticles

Subeen Shin

Department of Chemical Engineering

Graduate School of UNIST

Multi-color Upconversion Luminescence Tuning by Thermal Process with Silica Nanoparticles

A thesis/dissertation
submitted to the Graduate School of UNIST
in partial fulfillment of the
requirements for the degree of
Master of Science

Subeen Shin

01/03/2018 of submission
Approved by

01/21/13

Advisor
Jiseok Lee

Multi-color Upconversion Luminescence Tuning by Thermal Process with Silica nanoparticles

Subeen Shin

This certifies that the thesis/dissertation of Subeen Shin is approved.

01/03/2018 of submission

signature

01/21/18

Advisor: Jiseok Lee

signature

Sang Kyu Kwak : Thesis Committee Member #1

signature

Seok Ju Kang : Thesis Committee Member #2

Abstract

Multicolor luminescence tuning of upconversion nanocrystals (UCNs) is important to realize efficient photon upconversion for versatile applications ranging from bioimaging to encoding systems. Commonly used luminescence emission tuning methods, however, is limited by the complex synthetic process with precise stoichiometric control of lanthanide dopants. Here, we describe a novel macro-synthesis method of in which SiO_2 nanoparticles involved sintering process influences the inter-atomic distance to simultaneously manipulate the crystal phase (hexagonal to apatite), and multi-color luminescent efficiency of the UCNs. In the presence of SiO_2 nanoparticles, the hexagonal-to-apatite phase transition accompanies the color transition from yellow to green with high luminescence property, however, the hexagonal-to-cubic phase transition without SiO_2 nanoparticles raised to color transition from yellow to red which is weak and invisible under near-infrared light. Through this SiO_2 nanoparticles assistance, we also observed luminescence enhancement after a sintering process. These effects are explained by DFT calculation. We show that emission wavelength of UCNs can be manipulated through crystal phase transition with the change of SiO_2 NPs (nanoparticles) concentration and sintering temperature. Our results demonstrate potential application for covert multi-level security (MLS) system, including multi-colored emissive upconversion microcrystals (UCM) fabrication.

Contents

List of Figure

monomer solution with and without SiO_2 nanoparticles. (b) Emission spectra comparison of $NaGdF_4$ with and without SiO_2 nanoparticles

Figure 9. Comparison of UCNs embedded microstructures color transition with and without SiO_2 nanoparticles depending on the sintering temperature from 300~900 ℃ (a),(c) Normalized emission spectra of UCNs embedded microstructures without and with SiO_2 nanoparticles depending on the temperature. (b), (d) Color transition of UCNs without and with SiO_2 nanoparticles depending on the temperature.

Figure 10. Comparison of UCNs embedded microstructures color transition with the concentration of SiO_2 nanoparticles after annealing at 900 ℃ (a) Absolute emission spectra of UCNs embedded microstructures dependening on the concentration of SiO_2 ranged 5 ~ 60% (the ratio of SiO_2 and UCNs) (b) Normalized emission spectra of UCNs embedded microstructures depending on the concentration of SiO_2 through sintering process at 900 ℃ (c) UCNs embedded microstructures luminescence images depending on the concentration of SiO_2. (d) UCNs embedded microstructures luminescence images depending on the concentration of SiO_2 through sintering process at 900 ℃.

Figure 11. Comparison of absolute emission spectra of UCNs embedded microstructures through sintering process at 900 ℃. Emission spectra of sintered UCNs embedded structures with SiO_2 (Green line) and without SiO_2 (Red line)

Figure 12. Reflectance of UCNs (Powder) via UV-visible-NIR (Solid) spectrometer at room temperature. UCNs before sintering process (Black line), UCNs after sintering without SiO_2 nanoparticles (Red line) and SiO_2 assisted UCNs after sintering with SiO_2 nanoparticles (Green line)

Figure 13. Characterization of sintered UCNs embedded microstructures with SiO_2 nanoparticles (green color) (a) RGB value of SiO2 assisted UCNs embedded structures after sintering process at 900 ℃ (b) Mean RGB pixel value and Std.Dev of sintered UCNs embedded microstructures.

Figure 14. Characterization of sintered UCNs embedded microstruture with SiO_2 nanoparticles (green color) (a) Mean length of sintered UCNs embedded microstruture (Number of UCNs embedded structures = 100) (b) Comparison of TGA of UCNs integrated monomer solution with and without SiO_2 nanoparticles and SiO_2 nanoparticles

Figure 15. Comparison of absolute emission spectra of UCNs embedded microstruture as $NaGdF_4$:

Yb,Tm (18/0.2mol%) (a) Emission spectra of blue color emissive UCNs embedded microstruture before sintering (b) Emission spectra of blue color emissive UCNs embedded microstruture after sintering process at 900 ℃.

Figure 16. The averaged distance distribution of Er^{3+} ions by calculating the radial distribution function (RDF) of rare earth (RE) ion by using the DFT dynamics simulation

Figure 17. The proposed energy diagram of three types of phase crystals (hexagonal, cubic, and apatite)

Figure 18. Comparison of the structure and morphology transition of UCNs embedded microstruture depending on sintering temperature.

Figure 19. Comparison of FT-IR analysis of UCNs before and after sintering process at 900 ℃ (a) UCNs without SiO_2 nanoparticles before sintering (b) UCNs with SiO_2 nanoparticles before sintering (c) UCNs without SiO_2 nanoparticles after sintering (d) UCNs with SiO_2 nanoparticles after sintering

Figure 20. XRD pattern of UCNs with SiO_2 nanoparticles depending on the sintering time ranged from 15~120 min**.**

Figure 21. XRD pattern of UCNs without SiO_2 nanoparticles depending on the sintering temperature

Figure 22. XRD pattern of UCNs with SiO_2 nanoparticles depending on the sintering temperature ranged from 300~900 ℃

Figure 23. Comparison of the structure and morphology transition of UCNs embedded microstructures depending on sintering temperature. (a) Bio-TEM analysis (b) High-power powder XRD (c) High resolution TEM (HR-TEM)

Figure 24. Comparison of the structure and morphology transition of UCNs embedded microstructures depending on sintering temperature. (a) Bio-TEM analysis (b) High-power powder XRD (c) High resolution TEM (HR-TEM)

Figure 25. Comparison of the structure and morphology transition of UCNs embedded microstructures (a) Bio-TEM analysis (b) High-power powder XRD (c) High resolution TEM (HR-

List of Table

Nomenclature

UCNs	Upconversion nanoparticles
UCM	Upconversion Microcrystals
SiO_2 NPs	Silica nanoparticles
SEM	Scanning electron microscopy
HR-TEM	High-resolution transmission electron microscopy
XRD	X-ray diffraction
FT-IR	Fourier-transform infrared spectroscopy
TGA	Thermo gravimetric analysis
EDS	Energy dispersive spectrometer
MLS	Multi level security system

I. INTRODUCTION

1.1 Upconversion nanocrystals

The Luminescence material is a substance that emits light with the energy of visible light from the excitation source. Typically, there are down-conversion luminescent materials and upconversion nanocrystals. Downconversion nanoparticle (DCN) is an interactive luminescence process of photons converted to two low-energy photons such as organic dyes (Nat Med 9 (2003), pp. 112-117) and quantum dots (QD) (AP Alivisatos, Science, 1996, 271, 933-937). In contrary, upconversion nanoparticles (UCNs) are composed of multiphoton absorption process which emits short wavelength light emission with a long wavelength excitation source using an anti-stock process (F. Auzel, Chem. Rev. 2004, 104, 139 ., E. Downing et al., Science 1996, 273, 1185). The emission wavelength of the downconversion nanoparticle is longer than the excitation wavelength, the emission wavelength of the upconversion nanoparticle is shorter than the external energy (**Figure 1**, B. Zhou, Nat. Nanotechnol., 2015, 10, 924-936). In particular, the lanthanide doped nanocrystals are typical upconversion nanomaterials that convert to visible light in the near-infrared source (980 nm). An example of a lanthanide material is trivalent lanthanide ions, which are Gd^{3+}, Yb^{3+}, Er^{3+}, and Tm^{3+} having many electrons in the 4f orbital, followed by a multi-photon excitation process. In conventional, the Yb^{3+} ion (donor) absorbs energy at a wavelength of 980 nm and transfer its energy to Er^{3+} or Tm^{3+} ions (activator). This lanthanide doped UCNs has high photochemical stability and low background auto-fluorescence, low toxicity and large anti-stokes shift. For these reasons, the upconversion nanomaterials attract much attentions in many applications such as displays, sensors, bioimaging, etc. Furthermore, UCNs are capable of multicolor light emission from a single wavelength source and developed various synthesis methods to obtain high-quality upconversion nanocrystals with the various phases such as hexagonal, cubic, tetragonal crystals. One of them, hexagonal phase of UCNs ($NaYF_4$) was well-known for any of the high-quality upconversion hosts. Recently, UCNs have been widely used for bioimaging and phototherapy because of low photodamage and autofluorescence.

Additionally, UCNs can also have various properties through the surface treatment by silica coating, oxidation, acrylation, and ligand exchange (**Figure 2,** M. Wang, G et al., Nanomedicine: NBM 2011; 7: 710-729). Hydrophobic oleic acid capped $NaYF_4$ is expanding its utility for biological applications using a surface treatment for silica coating. We also acknowledge that color adjustment and phase adjustment of upconversion nanocrystals are very important factors for these various applications.

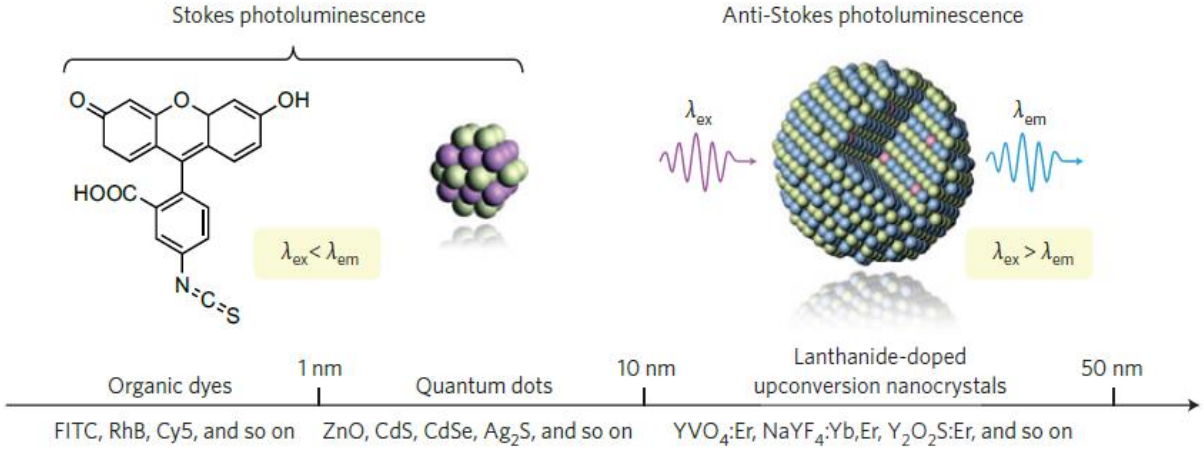

Figure 1. Representative downconversion and upconversion photoluminescence materials (B. Zhou et al., Nat. Nanotechnol., 2015, 10, 924-936)

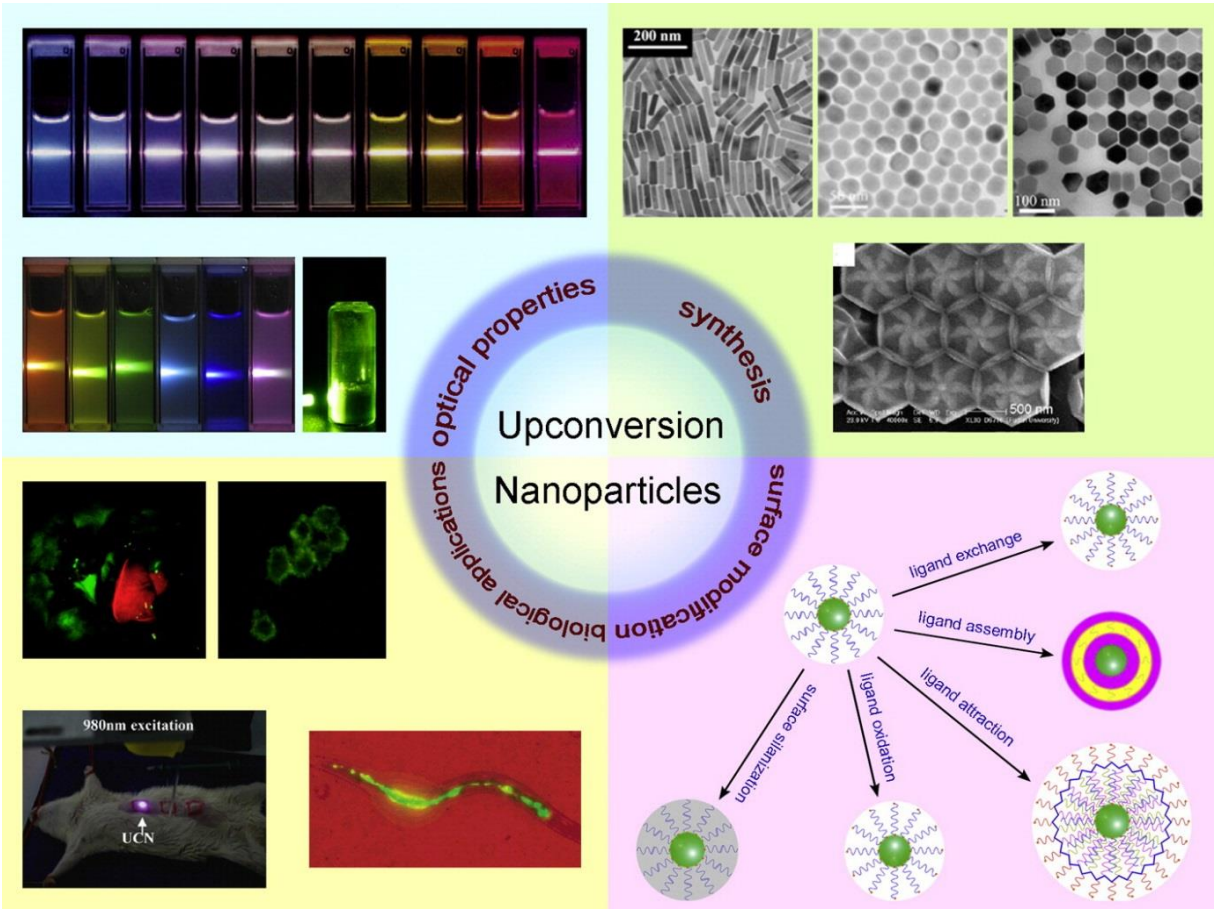

Figure 2. Upconversion nanoparticles properties (M. Wang, G et al., Nanomedicine: NBM 2011;7:710-729)

1.2 Upconversion nanocrystals background research

UCNs have been studied extensively for applications such as a photodynamic therapy (Niagara et al., Nature Medicine 18, 1580–1585, 2012), bioimagings (Liu et al., J. Am. Chem. Soc., 2011, 133 (43), pp 17122–17125), an UCNs ink of inkjet printer (You et al., Nanoscale, 2015, 7, 4423-4431), QR codes (Meruga et al., J. Mater. Chem. C, 2, 2221-222, 2014), and finger print for anti-counterfeit (M.Wang et al., Nano Res. 2015 June ; 8(6) 1800–1810), and display (F. Wang et al., Nature 463, 1061–1065, 2010) (**Figure 3**). In most cases, the color manipulating of UCNs is striking study and was conducted through the alkaline host controller (Zhang et al., Langmuir 2011, 27, 13236–13241), Mn^{2+} doping (Tian et al., Adv. Mater. 2012, 24, 1226–1231), and lanthanide ion control (Wang et al., J. AM. CHEM. SOC. 2008, 130, 5642–5643). Besides, UCNs had developed in varied morphology such as a cubic (Wang et al., J. AM. CHEM. SOC. 2008, 130, 5642–5643), hexagonal (F. Wang et al., Nature 463, 2010, 1061-1065), and tetragonal (Ding et al., CrystEngComm, 2013, 15, 6015–6021) (**Figure 4**).

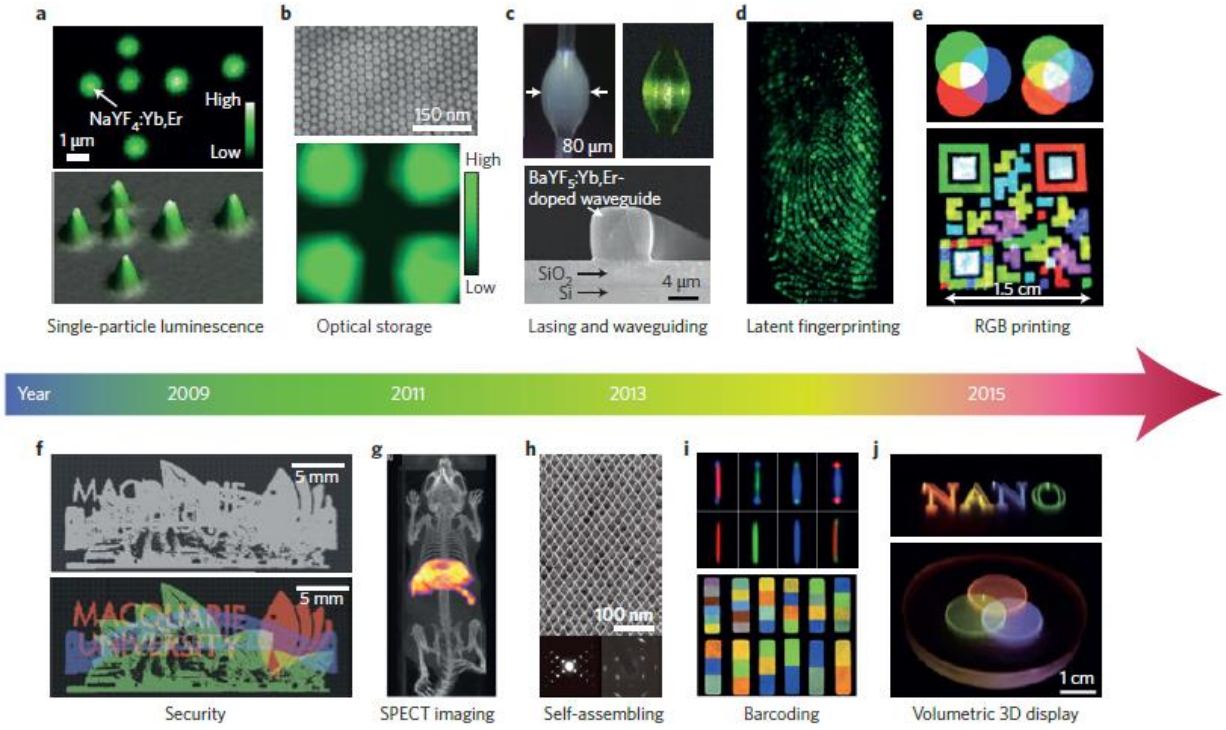

Figure 3. Selective milestones in multifunctionalization of upconversion nanoparticles for emerging applications. a, Confocal imaging of $NaYF_4$:Yb,Er nanoparticles at the single-particle level. b, Rewritable optical storage enabled by patterned NIR-lightresponsive nanoparticles. c, Lasing and waveguide amplifier using the nanoparticles as gain media. d, Latent fingerprinting through the use of $NaYF_4$:Yb,Er nanoparticles. e, Red–green–blue (RGB) printing involving nanoparticle inks. f,

Demonstration of document security printing, made possible by three sets of lifetime encoded $NaYF_4$:Yb,Tm nanoparticles. g, In vivo whole-body 3D imaging involving single-photon emission computed tomography (SPECT) through the use of 153Sm-radioactivated $NaLuF_4$:Yb,Tm nanoparticles. h, Self-assembly of fluoride-based nanoplates. i, Multicolour barcoding through single particles. j, Full-colour volumetric 3D display using pulse-duration-sensitive nanoparticles. (Zhou et al., Nature Nanotechnology 10, 924–936, 2015)

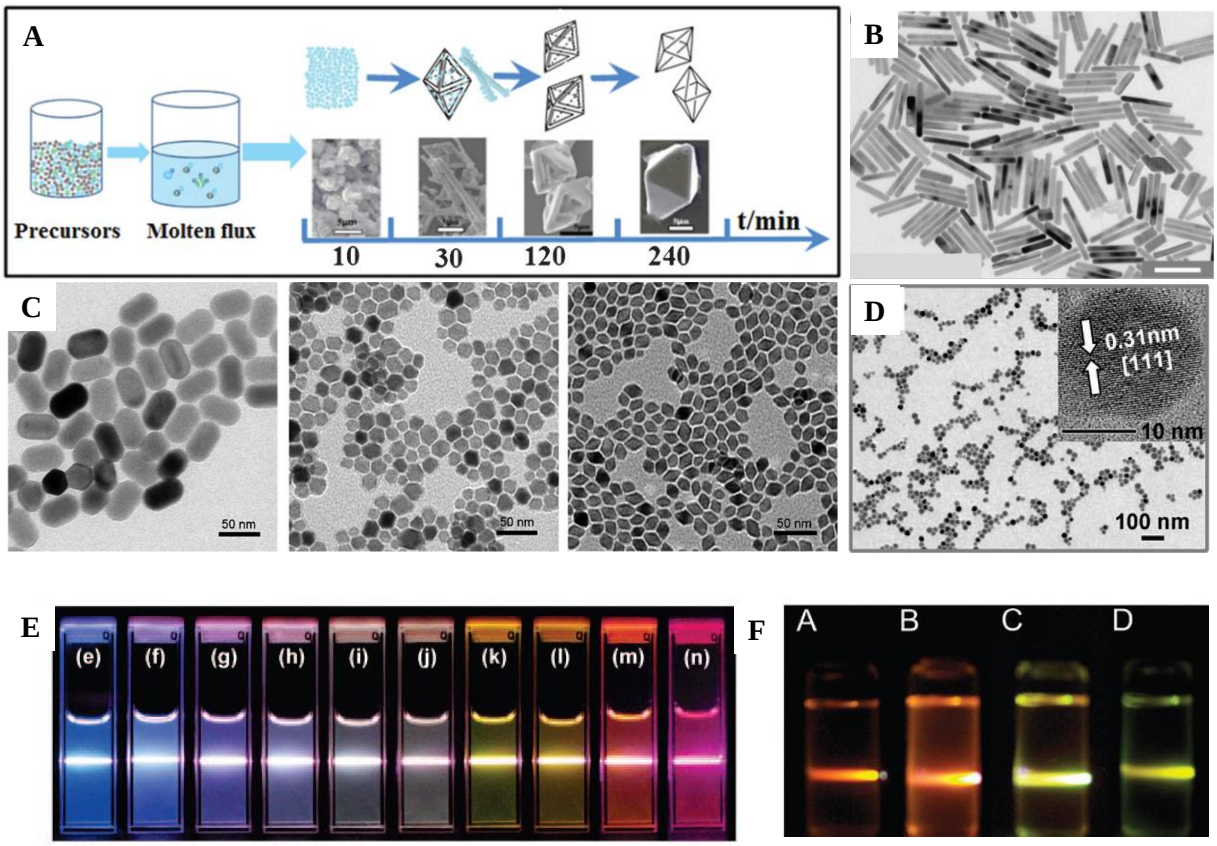

Figure 4. Diverse phase and color manipulating of Upconversion nanocrystals, a. Tetraogonal UCNs, b. Hexagonal rod shaped UCNs, c. Alkali doped UCNs, d. Cubic phase UCNs e, Lanthanide-doped multi-color UCNs, f. UCN color manipulation through reaction temperature.

1.3 Research Motivation

The emission color adjustment method shown in the above figure requires a complicated synthesis process involving accurate loading of the lanthanide dopants (Li et al., Nanotechnology 19, 2008, 345606) (Boyer et al., J. Am. Chem. Soc., 2006, 128 (23), p 7444- 7445) (Niu et al, J. Mater. Chem., 2010, 20, 9113-9117) and the limited materials to availble reactor for color tuning such as Ce^{2+} ion

doping (D. Chen et al., Journal of alloy sand compounds 654, 2016, 151-156), noble metal doping (Li et al., J. Phys . Chem. C 115 (8), p 3291 - 3296, 2011). In conventional, the emission color of UCNs depends on the inter-atomic distance between dopant ions such as Yb^{3+} and Er^{3+} (Wang et al., Nanoscale, 2013, 5, 3412 - 3420). **Figure 5** compares the emission color of the two phase of cubic and hexagonal. In the cubic system, the distance to Er^{3+} ions is close and the cross-relaxation easily occurs and as shown in the energy diagram, the red emission light dominantly appears due to this cross-relaxation. However, green emission is dominant because hexagonal UCN has a larger distance to Er^{3+} ions than cubic phase system. Therefore, we use silica nanoparticles as a novel former of upconversion nanomaterials (Shepherd et al., Adv. Mater 2008, 20, 4734-4739) to manipulate the color of UCN and fabricate dense and robust upconversion microcrystals with simultaneous color and phase transitions of UCNs and apply them to anti-counterfeit systems.

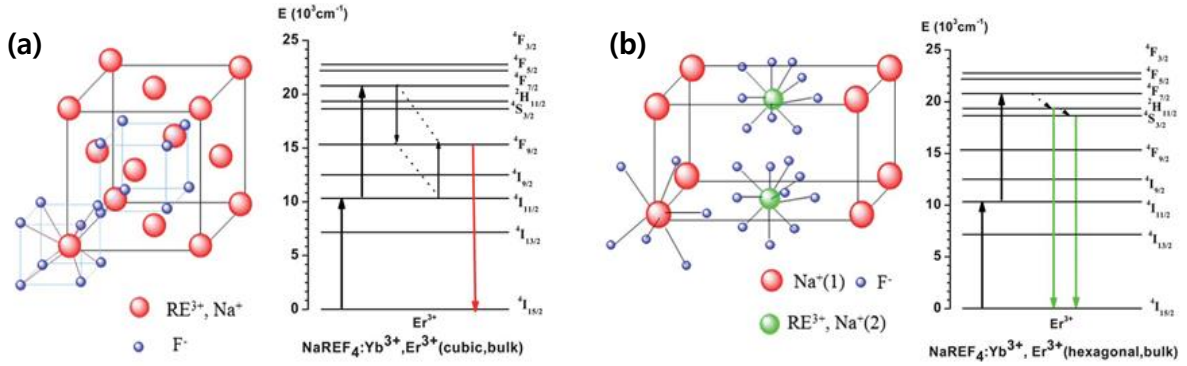

Figure 5. Schematic of phase structure and UCL processes and the cross-relaxation mechanisms in $NaREF_4:Yb^{3+}$, Er^{3+} under 980 nm excitation (a) Cubic (b) Hexagonal structure

1.4 Research Objective

In this research, we introduce a novel macro-synthesis method for multi-color luminescence transition of lanthanide doped UCNs with the incorporation of silicon dioxide. The interatomic distance between the lanthanide dopant was controlled by combining Si and O with UCNs host, and simultaneously, the emission color was changed through the sintering process. The resulting UC micro structure shows a dramatic multicolor transition that allows multi-spectral tuning capability. Extending the mixing of spectrally tuned UCNs to multiple colored luminescence and applying flow lithography technique to practical multi-level security (MLS) applications, it is possible to realize a luminescent color changeable microstructure with high physicochemical stability by this macro-synthesis method.

II. EXPERIMENTAL

2.1 Materials

All the chemicals used were purchased from Sigma-Aldrich without further purification. Silica nanoparticles (13 nm in diameter, US-nano), $GdCl_3 \cdot 6H_2O$ (Sigma-Aldrich, 99.999%), $YCl_3 \cdot 6H_2O$ (Sigma-Aldrich, 99.999%), $YbCl_3 \cdot 6H_2O$ (Sigma-Aldrich, 99.999%), $TmCl_3 \cdot 6H_2O$ (Sigma-Aldrich, 99.9%), NH_4F (Sigma-Aldrich, 99.9%), Oleic acid (Sigma-Aldrich, 90%), PUA (MINS-311 RM, Minuta tech.), cyclohexane (Sigma-Aldrich, anhydrous 99.5%), 2-hydroxy-2-methylpropiophenone (photo-initiator, Sigma-Aldrich)

2.2 UCNs synthesis (Hexagonal phase)

The hexagonal UCNs rods are synthesized by the hydrothermal method. The hydrothermal method is for the synthesis of single crystals under high temperature and pressure. The crystal growth is carried out in the steel pressure reactor called the autoclave and during the thermal reaction and cooling process, the crystal is grown. Briefly, NaOH (0.2 g ml^{-1}), oleic acid, ethanol, lanthanide solution mixture (0.2 M $RECl_3$) and ammonium fluoride (0.2 M NH_4F) was mixed during stirring for 10 min with specific stoichiometry. The emission color is manipulated by the concentration of lanthanide materials as shown table 1. In our research, we usually synthesized 4 colors of yellow, green, blue, and white. And then autoclaved at 200 ℃ for 3 hours to form crystal growth. After 3 hours, the resultant white color powder is washed to centrifuging with ethanol and water several times and dispersed in cyclohexane.

Mol %	Red	Orange	Yellow	Green	Covalt	Skyblue	Blue	Purple	White
Gd^{3+}	30	30	30	30	30	30	30	30	30
Y^{3+}			38	50	49.7	51.775	51.8		38
Yb^{3+}	69.9	68	30	18	20	18	18	69.7	31.7
Er^{3+}	0.1	2	2	2	0.1	0.025		0.1	0.1
Tm^{3+}					0.2	0.2	0.2	0.2	0.2

Table 1. Molar ratio of lanthanide dopant materials depending on the emission color

2.3 Synthesis of UCNs/SiO_2 embedded microstructure

UCNs and SiO_2 NP dispersed in photo-curable resin PUA/photo-initiator are flowed into PDMS microfluidic channel and polymerized by patterned UV (365 nm) light. We used polyurethane acrylate as the photo-curable resin to disperse UCNs well. To prevent the aggregation of UCNs in the photo-curable resin, the UCNs dispersed resin was processed using the ultra-sonication. Digital micro-mirror device (DMD) based maskless lithography technique was used to control the shape of microparticels. DMD could control the angle of micro-mirror and then micro-mirrors are tilted by an external signal. UCNs dispersed photo-curable resin flows into the microfluidic channel at 6.5 psi in pressure and then when the flow is stopped, the microparticle is synthesized immediately under 2 mW UV (365 nm) at 20 X objective. The microparticles are synthesized by three steps (stop-polymerization-flow) in cyclical fashions, therefore, we could synthesize high-throughput microparticles in short time. The synthesized microparticles were washed with ethanol to centrifuging at 1000 rpm for 5 s several times.

2.4 Fabrication of covert UC microstructure

By controlling the position of the stage with the LabView program, a covert microstructure including UCNs was synthesized. First, in order to fabricate a microarray, pretreatment was performed on a glass substrate through acrylate surface treatment. And then, the internal structure (triangle) is synthesized on the acrylated glass with 2 mW UV (365 nm) power and 100 ms exposure time. After synthesizing a single internal structure (triangle), the stage moves at a constant interval and speed to form a large area microarray structure. UV exposure time and a stage moving speed are controlled by turning on/off the LED light source and stage position with LabView (NI). Unpolymerized monomers are washed thoroughly with ethanol and then filled with a resin in which SiO_2 and UCNs are dispersed on the synthesized internal array structure to synthesize the external structure (circle) surrounding the internal structure, followed by polymerization of the circle structure under the same conditions of 2 mW UV power and 100 ms exposure time. Finally, the unpolymerized monomer was washed several times with ethanol.

2.5 Sintering Process

The synthesized UCNs/SiO_2 nanoparticles embedded microparticles or covert structure were dropped onto the sapphire windows (1 x 1 cm^2) and sintered at desired temperature (30 ℃ min^{-1}) under continuous air (mixture of 80% N_2 and 20% O_2) flow (20cm^3) for an hour in the tube furnace. After reaction, the sample is cool down to room temperature.

2.5 Imaging Condition

The emissive microstructure has luminescence property under near-infrared laser (980 nm, MDL-F-980-5W, PSU-H-LED) at 2 W. Before the annealing process, synthesized microstructures was dropped onto slide glass with imaging solution which is 10% polyethylene glycol 200 (PEG 200) in ethanol and then covered with glass. We used Nikon D-810 camera for color-imaging (shutter speed at 0.05 s) at 20 X objective and UCL emission spectra is recorded using a spectroscopy (QEPRO-FL, Ocean Optics) under 2 W NIR exposure. When measured NIR emission spectra, we cut off NIR range spectra using the IR filter (740 nm - cut off). After thermal process, the annealed microstructure included sapphire window was placed on IR cut-off filter onto microscope stage, and then NIR exposure at sapphire window and emission was represented.

2.6 Characterization

The crystal phase of the products were investigated by powder high-power X-ray diffraction (XRD) with D/MAX2500V/PC (Rigaku) with Cu Kα radiation (λ = 1.5418 Å) with an operation voltage and current maintained at 40 kV and 200mA. UCNs powder was filled on 5 mm XRD holder. Thermogravimetry analysis (TGA) measurements was carried out on a Q-500 (TA) at a heating rate of 10 ℃ min^{-1} over the temperature range of 50-900 ℃ under an air flow. The morphology of the samples were examined using a scanning electron microscope (SEM, S-4800, Hitach High-Technologies) with pre-treatment by Pt-coating of sample. Bio-transmission electron microscopy (Bio-TEM) were carried out on a JEOL JEM-1400 instrument with a field-emission gun operating at 120 kV and high-resolution transmission electron microscopy (HR-TEM) were carried out on a JEOL JEM-2100F instrument with a field-emission gun operating at 200 kV to examine the crystalline property of UCNs and diffraction pattern. Fourier transform infrared (FT-IR) spectroscopy was carried on a Varian and measures the IR absorbance to determine vibrational frequency which provides Si-O-Si chemical bonding with spectral range from 4000 ~ 50 cm^{-1} and ATR. UV-visible-NIR spectroscopy (Solid) was carried out on a Cary-5000 in the wavelength range from 200 ~ 3,300 nm for reflectance measurement with PMT detector.

2.7 Simulation details

We used the discrete dipole approximation (DDA) calculation to investigate the difference of luminescence intensity of UCN depending on the existence of silica nanoparticles (SiO_2 NP). Additionally, we conducted the density functional theory (DFT) calculation to investigate the structural and electronical characteristics of three phases (i.e., hexagonal, cubic, and apatite phases).

III. RESULTS & DISCUSSION

3.1 Experimental Design

Firstly, hexagonal UCNs is synthesized using the previously reported hydrothermal method. (Wang et al., Nature 463, 1061-1065). Briefly, **Figure 6** shows that the SiO_2 nanoparticle assistance brings the phase transition and color change of UCNs. Silica nanoparticles could be selected as a precursor for color adjustment of UCNs, because they have dissolution properties into the host material and the crystal size is small. The synthesized $NaGdF_4$:Yb/Er (30/2 mol%) has a hexagonal phase, where the addition of amorphous SiO_2 nanoparticles increases the unit lattice volume of $NaGdF_4$ during the thermal process. As a result of the hexagonal phase transition to apatite causes Er^{3+} ions in the UCNs lattice to increase in volume due to substitution with silica nanoparticles. The increase in the distance of Er^{3+} ions generated simultaneously with the phase transition and resulted in a change in color from yellow to green. Furthermore, the apatite phase transition from hexagonal also showed excellent light stability. However, in the absence of SiO_2 nanoparticles, the change in the crystal structure of $NaGdF_4$ changes to cubic crystal, and the volume of the unit cell decreases. This phase transition to cubic accompanies a remarkable decrease in emission intensity and shows a change in color of red emission which is invisible to the naked eye under 980 nm near-infrared light.

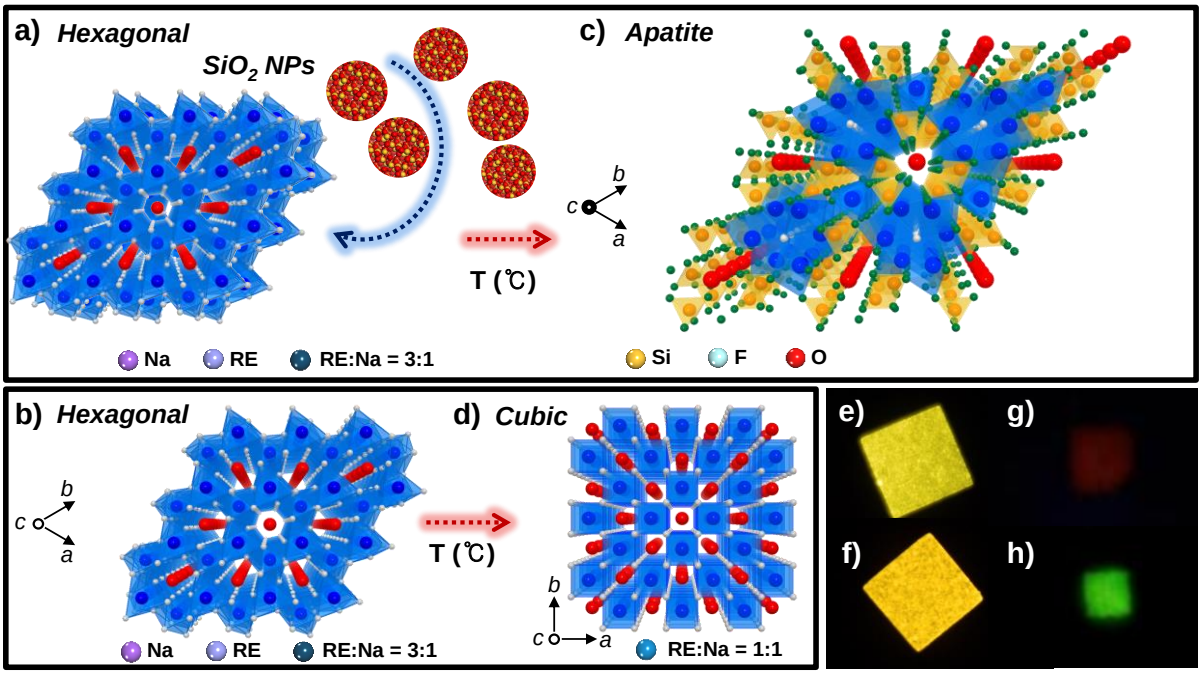

Figure 6. Schematic diagram of phase and color transition of $NaGdF_4$ with sintering process (a), (c), (e), (g) Silica nanoparticles assisted hexagonal-to-apatite phase transition (b), (d), (f), (h) Hexagonal-to-cubic phase transition induced color change.

3.2 Characterization of UCNs and SiO_2 nanoparticles

The characterization of UCNs was examined through HR-TEM, SEM, XRD, and EDS mapping. UCNs synthesized as prepared method have hexagonal phase rod shape at 300 nm in length and 70 nm in width as shown SEM image and XRD pattern (**Figure 7a~c**). Amorphous SiO_2 nanoparticles have 13 nm in diameter. Yellow emissive UCNs as $NaGdF_4$: Yb/Er (30/2 mol%) has doped lanthanide atom as Y^{3+}, Gd^{3+}, Yb^{3+}, and Er^{3+} examined by EDS mapping (**Figure 7d**). Oleic acid capped UCNs has the hydrophobic surface and then dispersed well in urethane monomer solution.

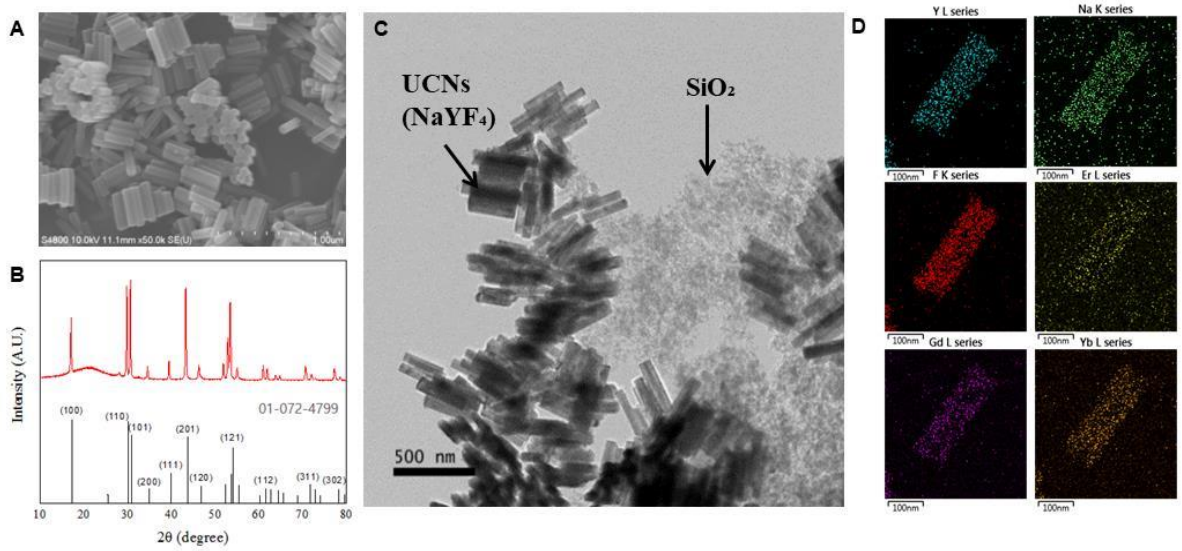

Figure 7. Characterization of UCNs with SiO_2 nanoparticles. (a) SEM image of $NaGdF_4$: Yb, Er (30/2%) (b) Powder-HPXRD of $NaGdF_4$:Yb, Er (30/2%) (c) HR-TEM image of $NaGdF_4$: Yb, Er (30/2%) with SiO_2 nanoparticles (d) EDS mapping of $NaGdF_4$: Yb, Er (30/2%) doped Y^{3+}, Yb^{3+}, Gd^{3+}, and Er^{3+}.

3.3 Effect of SiO_2 nanoparticles integrated UCNs

To investigate the influence of SiO_2 nanoparticles on UCNs, four types of UCNs, yellow, blue, green and white, were fabricated and dispersed well in a liquid monomer solution (PUA). UCNs dissolved monomer solution is transparent to the naked eye, but the solution in which the UCNs and SiO_2 nanoparticles are dispersed is opaque due to the scattering effect of the small size silica nanoparticles (**Figure 8a**). In the spectra result, a very bright emission band of 550 nm and 650 nm appears in the synthesized yellow emission UCNs. Interestingly, the luminescence intensity of the UCNs microstructure containing SiO_2 is two times higher than in the absence of SiO_2 nanoparticles (**Figure**

8b). We estimate that the positive effect of the presence of SiO_2 nanoparticles on upconversion luminescence efficiency is due to the increase in the photon absorption of UCNs due to the scattering effect of SiO_2 nanoparticles. By scattering effect of SiO_2 nanoparticles, increase of photon absorption rate of monomer with UCN dispersed is calculating by simulation. Therefore, we found that SiO_2 nanoparticles are an important factor to further enhancement of upconversion emission intensity by scattering effect.

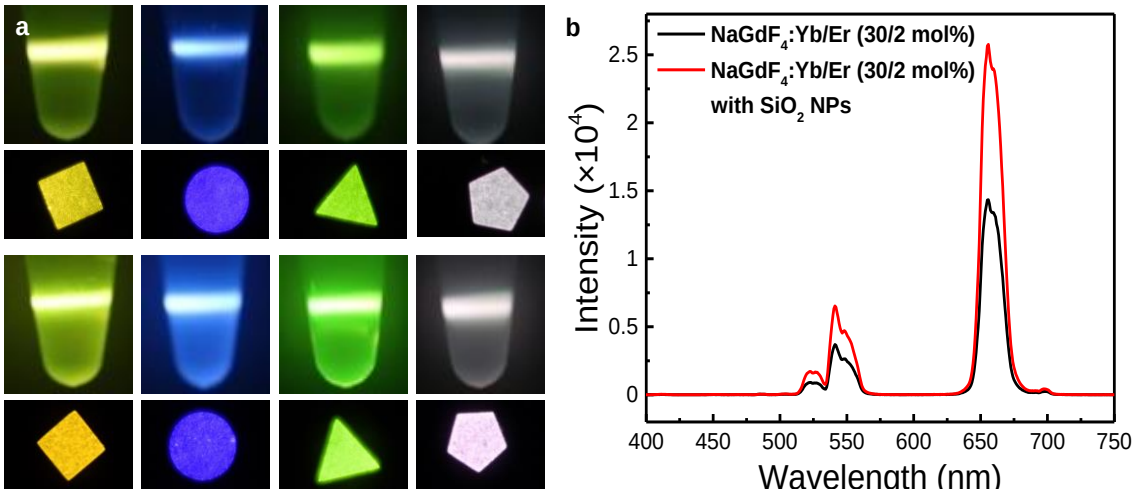

Figure 8. The effect of SiO_2 nanoparticles assisted UCNs (a) Luminescence comparison of UCNs in monomer solution with and without SiO2 nanoparticles. (b) Emission spectra comparison of $NaGdF_4$ with and without SiO_2 nanoparticles

3.4 Color transition of UCNs embedded structures through sintering process

First, we explored the temperature effect of luminescent color conversion of UCNs when adding silica nanoparticles. Based on the presence of SiO_2, after sintering with increasing temperature, different color transition tendency was predominantly observed (**Figure 9)**. UCNs embedded microstructures showing yellow light emission were found to have a small volume shrinkage and a color transition to orange emission after sintering at 300 ℃. We believe that the change in color from yellow to orange is due to the carbonized polymer matrix. This result was proved that the sharp weight decrease where the PUA resin disappeared completely at 500 ℃ from the TGA data (**Figure 14**). Therefore, the polymer matrix could be maintained at 300 ℃ and the color of microparticles showed optically red color, and the orange luminescent color showed reduced green emission intensity at 550 nm. After sintering at 900 ℃, the microparticles containing UCNs showed red

emission where the polymer matrix was completely consumed, the volume shrinkage was reduced to 50%, and the luminescence intensity was also sharply reduced. Interestingly, however, when SiO_2 nanoparticles were added, surprisingly the green peak intensity (550 nm) exceeded the red peak intensity (660 nm) after sintering at 900 ℃. Therefore, in the sintering process, the SiO_2 nanoparticles controlled the distance between the Er^{3+} ions which melted into the UCN host and realized a change in color from yellow to green. When comparing the emission intensities of the transition colors (red and green) after sintering, it was confirmed that the luminescence intensity increased by 2 orders of magnitude at 550 nm compared to those without SiO_2 (**Figure 11**). Additionally, to compare the emission efficiency of UCNs, the reflectance was measured by UV-visible-NIR spectroscopy. In this analysis, the difference between the emission spectrum and the color change was observed (**Figure 12**).

Besides, studies were conducted to change the ratio of SiO_2 and UCNs (**Table. 2**) to control the emission properties with the concentration of SiO_2 nanoparticles. Before the annealing process, it was found that the initial yellow emission intensity gradually increases as the concentration of the silica nanoparticles increases. This result is due to the scattering effect which causes an increase in photon absorption efficiency under NIR source, as described in **Figure 7**. After annealing, when the silica concentration increases from 5% to 60%, the color transition gradually changes from red to green, and correspondingly the green peak at 550 nm gradually increases (**Figure.10**). Dissolution efficiency is different depending on the amount of SiO_2 nanoparticles, and the extent of controlling the distance to Er^{3+} ions is also different. Therefore, by manipulating the concentration of SiO_2 nanoparticles, it was possible to control the transition color as atomic distance control and we were able to expand the realization range of color. In addition, the RGB values of the obtained green UC microstructure were measured to confirm the homogeneity of the annealed color, and after annealing, the distribution of the length of the microparticle (**Figure 14**) was also measured.

Furthermore, we observed the change in color before and after annealing of UCNs that emits blue color, however, the transition color was the same as blue but the difference in emission intensity was able to be confirmed (**Figure 15**). In this way, we believe that the color change also depends on the type of activator dopant. When the Er^{3+} activator is doped into UCNs, the releasable colors are red, orange, yellow and green, thus, we could control the color transition from red to green gradually by manipulating the distance between Er^{3+} ions with the SiO_2 nanoparticles. The higher the concentration, the larger the distance between Er^{3+} ions gradually increases during the annealing process, and the color can transition from red to green. However, since the Tm^{3+} ion doped color is exclusively blue, there is almost no difference in color conversion due to SiO_2, which is the only possible transition color in blue. However, silica has the property of amplifying the luminescence intensity of UCNs, the difference of the luminescent intensity appears.

Additionally, the volume change of SiO_2 nanoparticles was also investigated from TGA data during the thermal process. In this graph, we have found that the mass of SiO_2 nanoparticles is nearly constant after heat treatment at 900 ℃. For this reason, we assume that the SiO_2 nanoparticles do not disappear during the heat treatment process, but after being dissolved in the UCNs material, it will form another structure with the phase transition. Thus, the SiO_2 nanoparticles could be precursors of the phase transition and novel network formers of upconversion nanocrystals.

Therefore, we thought that color variation of UCNs is ultimately due to the phase transition, and in order to understand the color transition phenomenon according to interatomic distance, we have explored a cross-relaxation process by decreasing the distance of Er^{3+} ions. We calculated the rare earth (RE) ion radiation distribution function (RDF) using DFT dynamic calculation and investigated the average distance distribution of Er^{3+} ions. In **Figure 16**, as the number of RE^{3+} ions increases according to the radial distance of the RE^{3+} ions, the distance between them is shorter and the cubic crystal dominates than the hexagonal and the apatite crystal structure. This shows that the cubic has a relatively high cross-relaxation like the proposed energy diagram (**Figure 17**) and realizes the red emission color. Therefore, we confirmed that the main reason for simultaneous phase and color transitions of upconversion nanocrystals using SiO_2 nanoparticles is the distance between the atoms of Er^{3+} ions in each crystal phase.

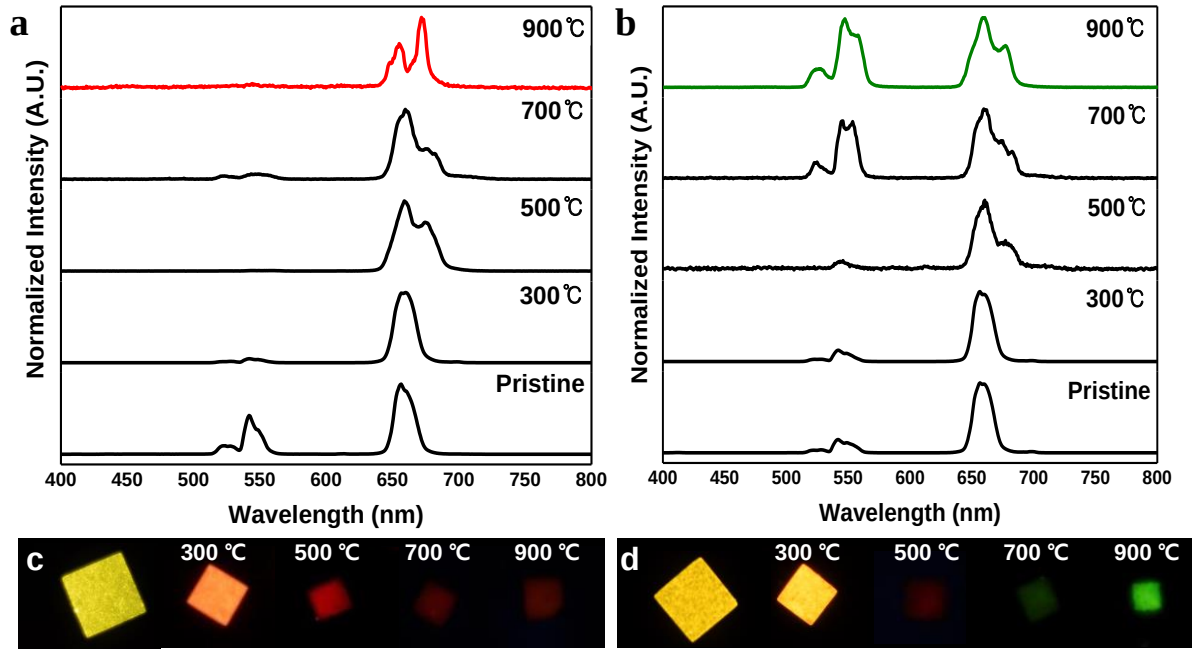

Figure 9. Comparison of UCNs embedded microstructures color transition with and without SiO_2 nanoparticles depending on the sintering temperature from 300~900 ℃ (a),(c) Normalized emission spectra of UCNs embedded microstructures without and with SiO_2 nanoparticles depending on the temperature. (b), (d) Color transition of UCNs without and with SiO_2 nanoparticles depending on the temperature.

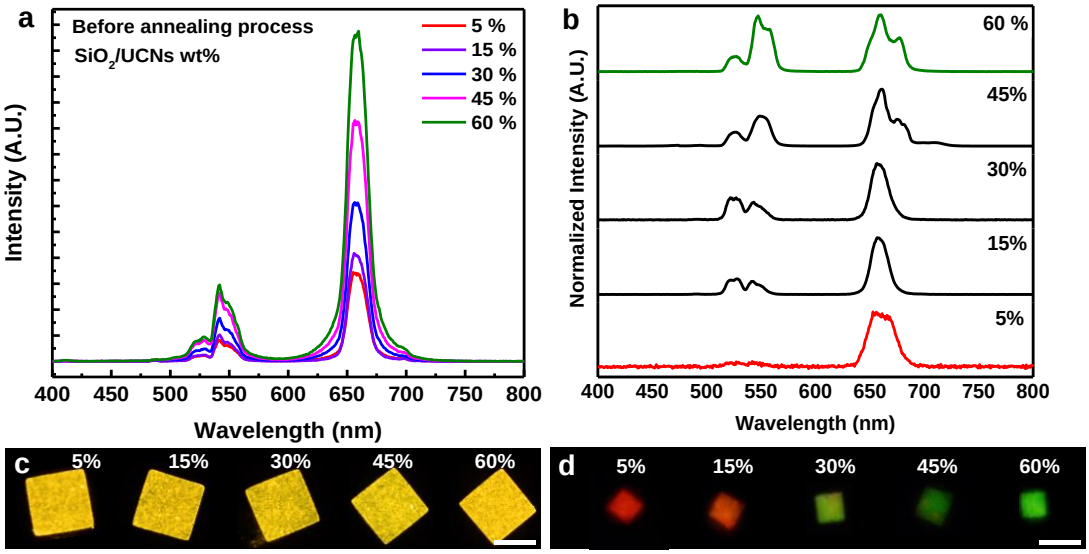

Figure 10. Comparison of UCNs embedded microstructures color transition with the concentration of SiO_2 nanoparticles after annealing at 900 ℃ (a) Absolute emission spectra of UCNs embedded microstructures dependening on the concentration of SiO_2 ranged 5 ~ 60% (the ratio of SiO_2 and UCNs) (b) Normalized emission spectra of UCNs embedded microstructures depending on the concentration of SiO_2 through sintering process at 900 ℃ (c) UCNs embedded microstructures luminescence images depending on the concentration of SiO_2. (d) UCNs embedded microstructures luminescence images depending on the concentration of SiO_2 through sintering process at 900 ℃.

SiO_2/UCNs	5%	15%	30%	45%	60%
SiO_2 (mg)	3	9	18	27	36
UCNs (mg)	60	60	60	60	60
PUA resin (μℓ)	540	540	540	540	540
Photo-initiator (μℓ)	60	60	60	60	60

Table 2. Concentration of UCNs and SiO_2 nanoparticles in PUA resin with photo-initiator

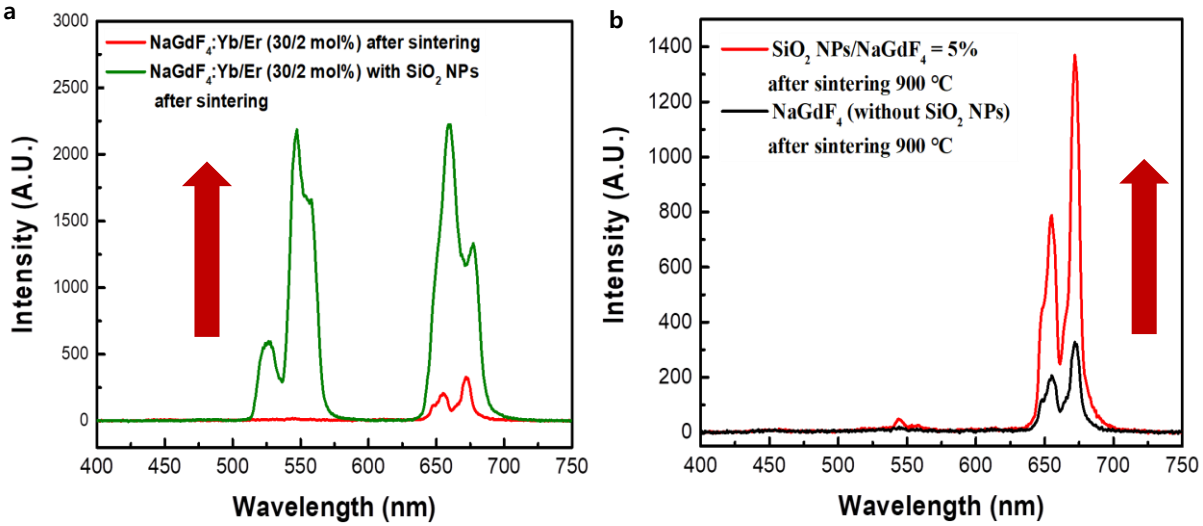

Figure 11. Comparison of absolute emission spectra of UCNs embedded microstructures through sintering process at 900 ℃. Emission spectra of sintered UCNs embedded structures with SiO_2 (Green line) and without SiO_2 (Red line).

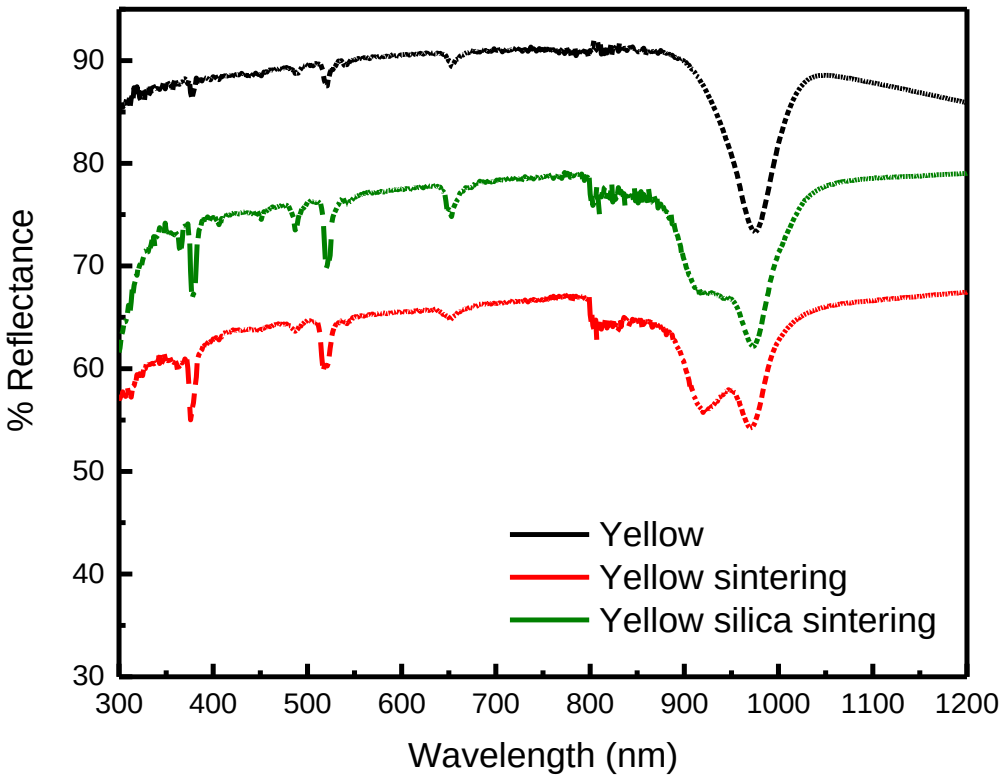

Figure 12. Reflectance of UCNs (Powder) via UV-visible-NIR (Solid) spectrometer at room temperature. UCNs before sintering process (Black line), UCNs after sintering without SiO_2 nanoparticles (Red line) and SiO_2 assisted UCNs after sintering with SiO_2 nanoparticles (Green line)

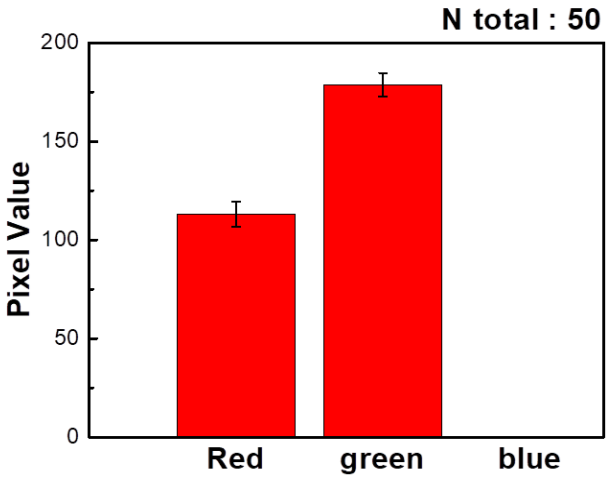

Figure 13. Characterization of sintered UCNs embedded microstructures with SiO_2 nanoparticles (green color) (a) RGB value of SiO2 assisted UCNs embedded structures after sintering process at 900 ℃

	N total	Mean	Std.Dev	Sum	Min	Median	Max
R	50	113.06	6.2447	5653	98	114	125
G	50	178.78	33.7	8939	162	179	190

Table 3. Mean RGB pixel value and Std.Dev of sintered UCNs embedded microstructures

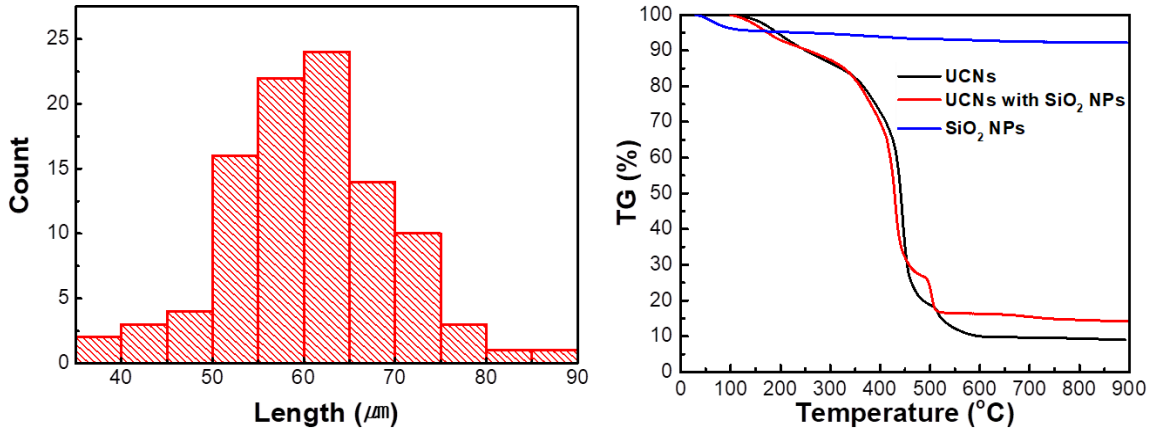

Figure 14. Characterization of sintered UCNs embedded microstructures with SiO_2 nanoparticles (green color) (a) Mean length of sintered UCNs embedded microstructures (Number of UCNs embedded microstructures = 100) (b) Comparison of TGA of UCNs integrated monomer solution with and without SiO_2 nanoparticles and SiO_2 nanoparticles

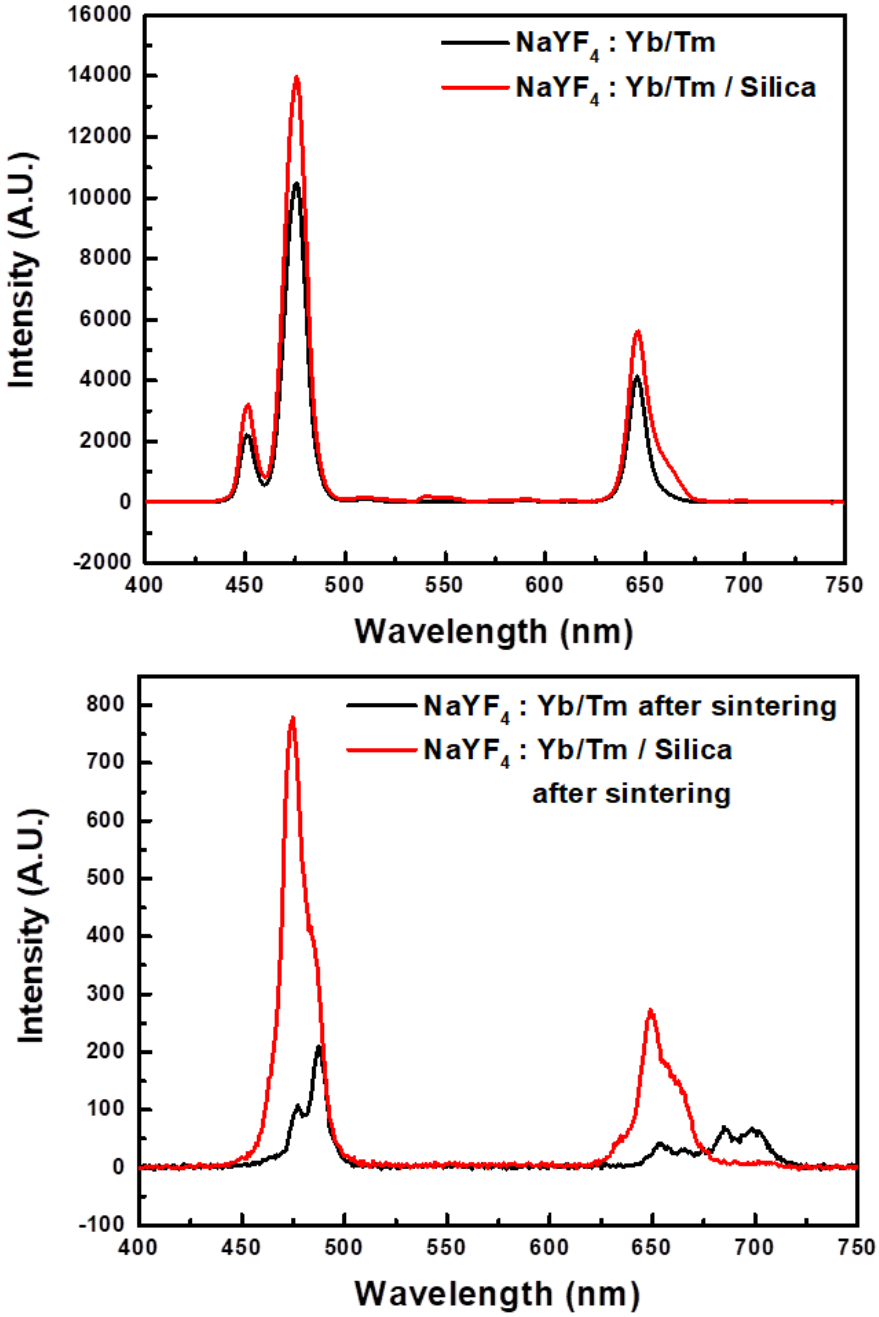

Figure 15. Comparison of absolute emission spectra of UCNs embedded microstructures as $NaGdF_4$:Yb,Tm (18/0.2mol%) (a) Emission spectra of blue color emissive UCNs embedded microstructures before sintering (b) Emission spectra of blue color emissive UCNs embedded microstructures after sintering process at 900 ℃.

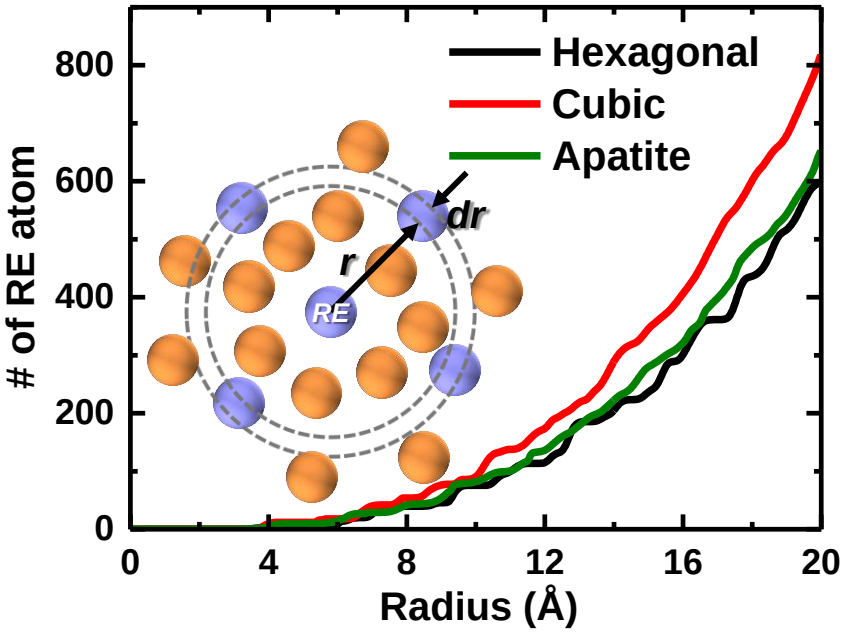

Figure 16. The number of rare earth (RE) atoms within the same distance from the reference RE atom, calculated by integration of the radial distribution function (RDF) of RE atoms for the three types of crystalline phase

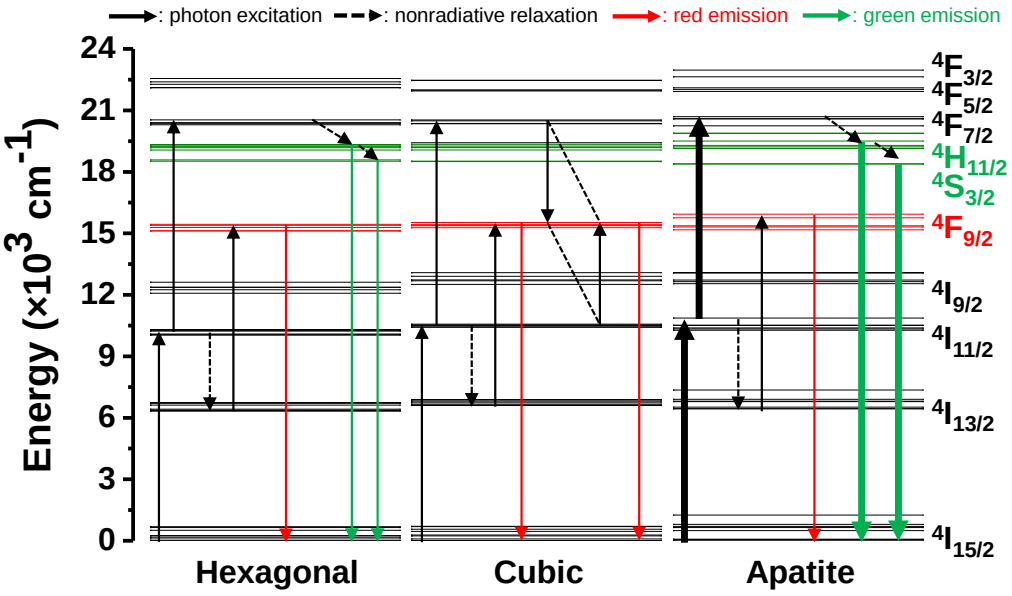

Figure 17. Proposed energy transfer mechanism of Er^{3+} ion according to the hexagonal, cubic, and apatite phases

3.5 Phase transition of UCNs embedded structures through sintering process

The emission color of UCNs depends on the distance to Er^{3+} ions as mentioned before. UCNs can emit various emission lights from green to red by changing the distance between Er^{3+} ions at a short distance from a long distance. In this study, powder X-ray diffraction (XRD), scanning electron microscope (SEM) and transmission electron microscope (TEM) analysis were performed to analyze the phase transition, which is the cause of color change.

First, we investigated the morphological change of microstructures containing UCNs and SiO_2 nanoparticles according to annealing temperature by SEM analysis (**Figure 18**). As for the microstructure containing only UCNs, it was confirmed that as the annealing temperature increased, the distance between the UC nanorods became close by the burning of the polymer matrix, and the volume of the microstructure decreased. By contrast, when SiO_2 nanoparticles are added to UCNs, the original structure has UCNs nanorods and spherical SiO_2 nanoparticles with a diameter of 10 nm, but as the annealing temperature increases, the distance of the nanorods approaches, the UC nanorods and SiO_2 nanoparticles aggregated with each other to form micro-crystals, it was impossible to observe the morphology of nanorod and nano-spherical material. Therefore, we were convinced that SiO_2 nanoparticles aggregate and dissolve in UCNs material during the sintering process. Through the Fourier Transform Infrared Spectroscopy (FT-IR) analysis, the reaction between the SiO_2 nanoparticles and UCNs in the annealing process was also confirmed (**Figure 19**). In the absence of SiO_2 nanoparticles, the peak of Si-O- Si bond was not shown at the wavelength of 900 cm^{-1}, but when SiO_2 nanoparticles were added to UCNs, the Si-O-Si bond was clearly confirmed and appears more pronounced after annealing process

After the thermal treatment, the phase transition was investigated while adjusting the annealing time from 15 minutes to 2 hours under continuous air flow in order to obtain stable crystal phase of UCNs (**Figure 20**). The phase transition started to appear at the reaction time of 15 minutes, and when it reached 1 hour, the XRD pattern was consistent with the apatite phase and had a very stable structure. However, when the annealing time exceeds 1 hour, the XRD pattern changes little by little again. Therefore, it was found that the reaction time is an important factor for phase transition of UCNs and formation of apatite phase crystal by a sintering process. Therefore, we conducted a research system for 1 hour overall.

The previous color transition study suggested that the various emission color ranging from green to red in conventional UCNs are strongly upon the distance between adjacent Er^{3+} ions. The characteristic color transition of our UCNs samples, therefore, indicates that the simple annealing process plays a critical role to control the lanthanide-atomic distance. The high-temperature thermal annealing process affords sufficient energy to change the phase of UCNs resulting in transition of

luminescence color and intensity. In order to quantitatively measure the exact role of thermal treatment, we further performed the various spectroscopy measurements including powder X-ray diffraction (XRD), scanning electron microscopy (SEM), cross-sectional transmission electron microscopy (TEM) analysis and selected area electron diffraction (SAED). We systematically sintered UCNs with and without SiO_2 by air purged tube furnace and subsequently cool down to room temperature to measure the XRD (**Figure 21~22**). The resulting out-of-plane XRD patterns as a function of sintering temperature with and without SiO_2 nanoparticles shows the characteristic of reflections at relatively low thermal annealing temperature exhibits similar patterns with strong and narrow (100), (110), (101) and (201) peaks (**Figure 23**), indicating the SiO_2 crystals are not significantly altered the crystal phase of UCNs because of insufficient energy for Si atom diffusion. In addition, the surface morphologies of individual sample analyzed by SEM implied the low sintering temperature is not sufficient to change the phase and shape of UCNs where the smooth surface of rectangular UCNs on Si substrate was well characterized for both with and without SiO_2 contained samples. The complementary cross-sectional TEM with SAED measurement also revealed that single crystal-like hexagonal texture of UNCs are mostly hexagonal $NaYF_4$ phase (JCPDS file number 01-072-4799) which is well matched with XRD results (**Figure 24**). In contrast, at high-temperature sintering treatment (700 to 900 ˚C), different crystal phases were clearly evidenced by XRD measurement where the characteristic reflections of UCNs without SiO_2 exhibits cubic $NaYF_4$ phase (JCPDS file number 01-077-2042), meanwhile the UCNs with SiO_2 shows $NaY_9Si_6O_{26}$ (apatite) phase (JCPDS file number 00-035-0404) (**Figure 25**). The different crystal phases are mainly due to the existence of Si atoms in SiO_2 nanoparticles on the UCNs are successfully diffuse into the UCNs resulting in evolved apatite crystal. In particular, SAED pattern of UCNs with SiO_2 exhibits representative reflections of (002), (012), (121) and (022) which are well matched with the expected reflection of apatite phase. Furthermore, we also found that the lattice fringe which means the high crystalline property of apatite phase of UCNs as shown high-resolution TEM (HR-TEM) images even the cases of the hexagonal and cubic phase of UCNs.

We also studied the multi-step annealing process continuously (**Figure 26**). First, a cubic crystal was obtained from hexagonal UCNs by thermal treatment at 900 ℃, then SiO_2 nanoparticles were added to this cubic phase and a secondary annealing process was carried out. Thr resultant crystal of multi-step annealing is consistent with single heat treated apatite crystals formed by direct annealing from hexagonal UCNs with SiO_2 nanoparticles. From this result, it was confirmed that the SiO_2 nanoparticles are precursors that generate apatite of UCNs after the high-temperature sintering process. However, when SiO_2 nanoparticles are heat treated without UCNs, the sintered phase is not an apatite phase, thus, SiO_2 nanoparticles could change the crystal phase of UCNs to apatite in any phase (**Figure 27**).

Finally, the phase transition with SiO_2 concentration was also studied (**Figure 28**). Even when only a small amount of SiO_2 is added to UCNs, the phase transition is shown after the sintering process and as the concentration of SiO_2 gradually increases, they approach the apatite structure, it changes from red to green with the distance change between the atoms.

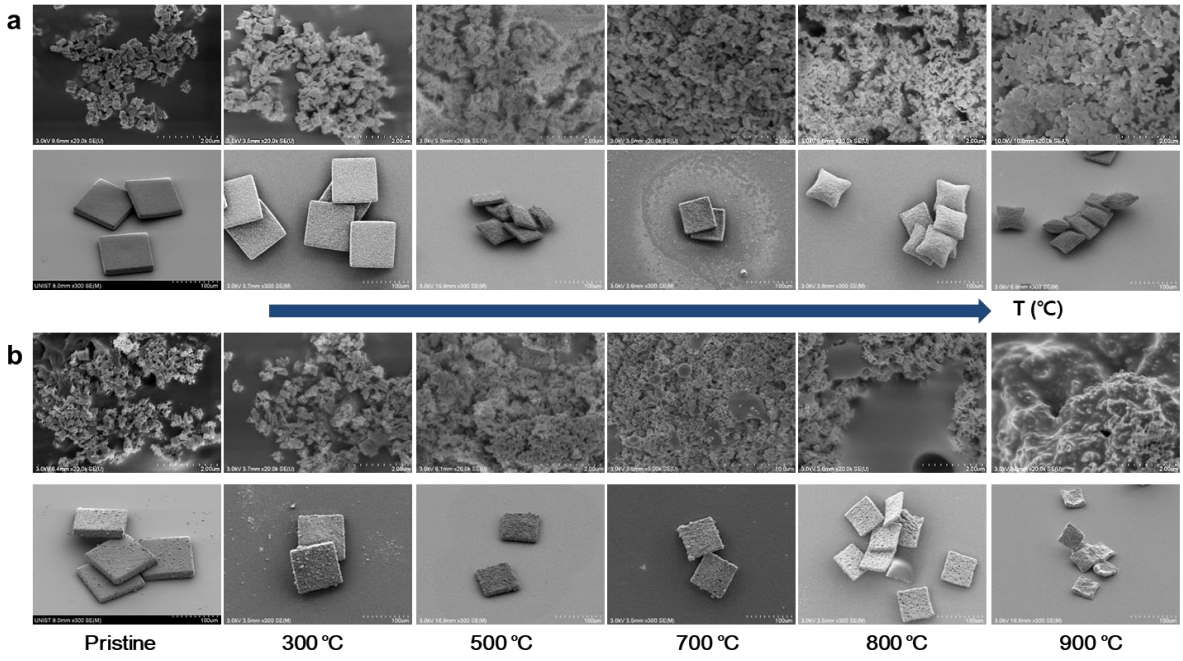

Figure 18. SEM images of UCNs embedded microstructures depending on the sintering temperature ranged from 300~900 ℃ (a) without SiO_2 nanoparticles (b) with SiO_2 nanoparticles

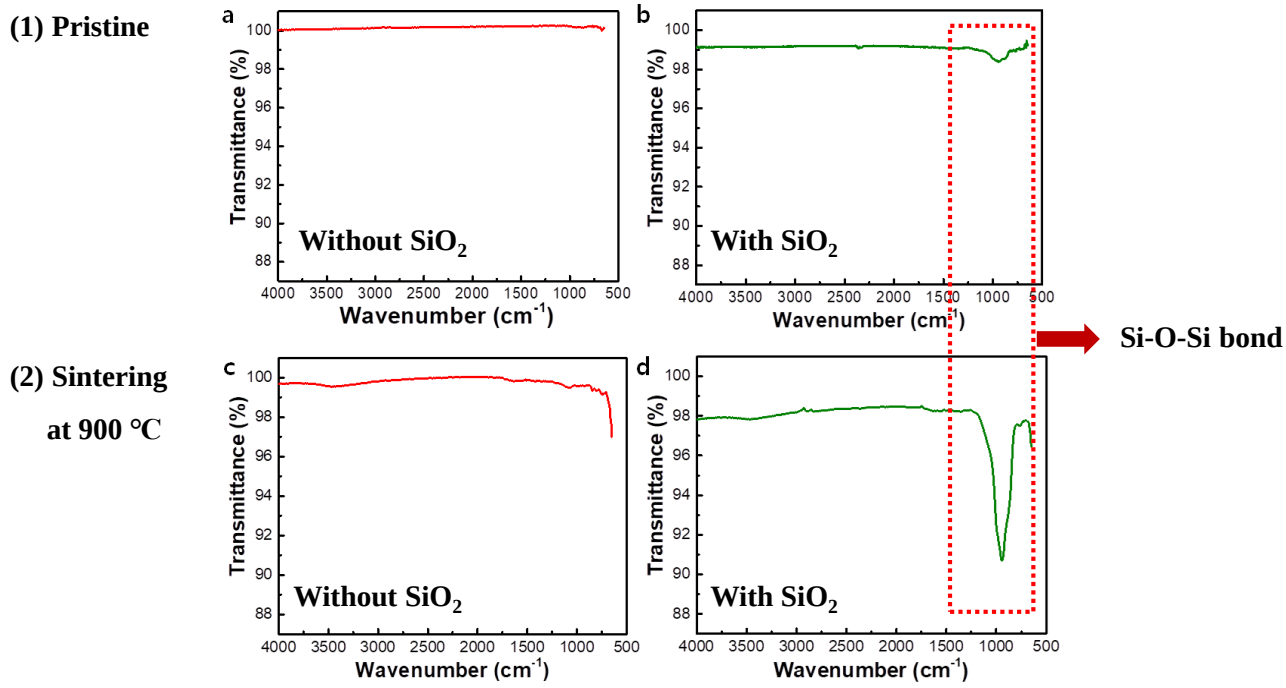

Figure 19. Comparison of FT-IR analysis of UCNs before and after sintering process at 900 ℃ (a) UCNs without SiO_2 nanoparticles before sintering (b) UCNs with SiO_2 nanoparticles before sintering (c) UCNs without SiO_2 nanoparticles after sintering (d) UCNs with SiO_2 nanoparticles after sintering

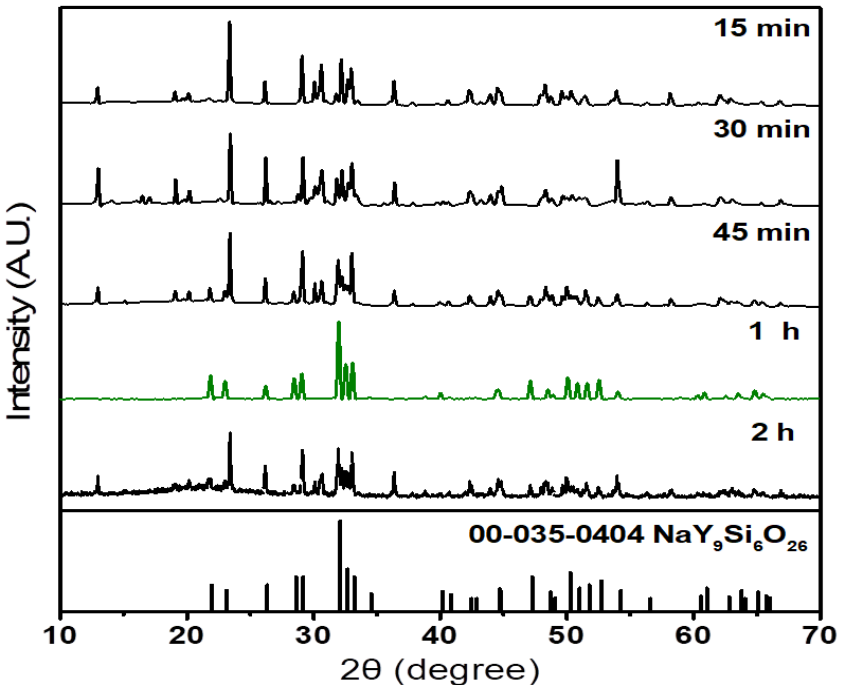

Figure 20. XRD pattern of UCNs with SiO_2 nanoparticles depending on the sintering time ranged from 15~120 min**.**

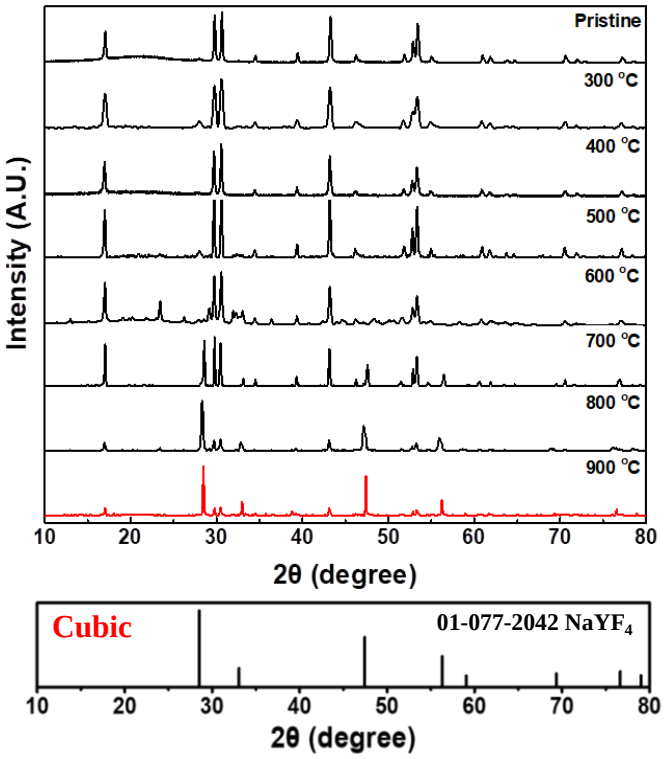

Figure 21. XRD pattern of UCNs without SiO_2 nanoparticles depending on the sintering temperature

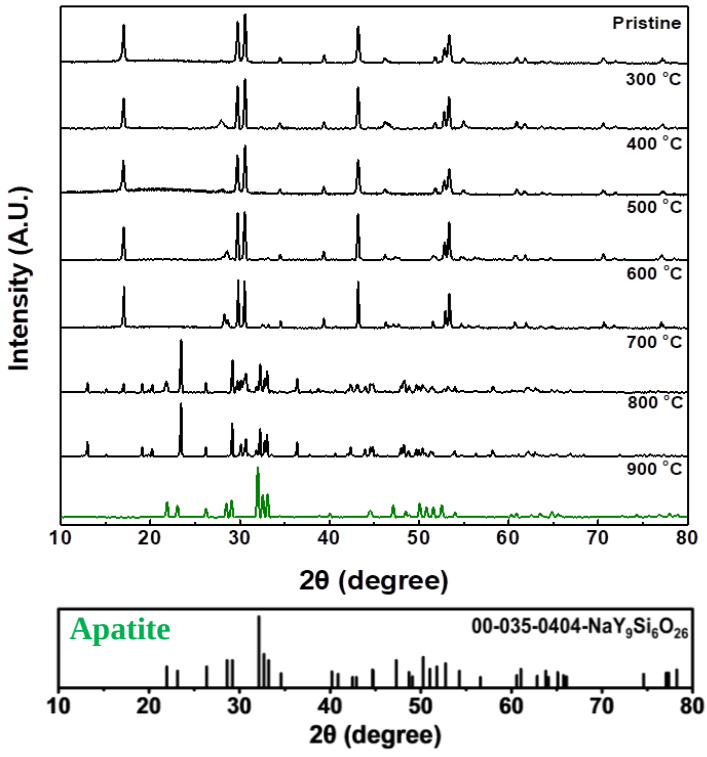

Figure 22. XRD pattern of UCNs with SiO_2 nanoparticles depending on the sintering temperature ranged from 300~900 ℃

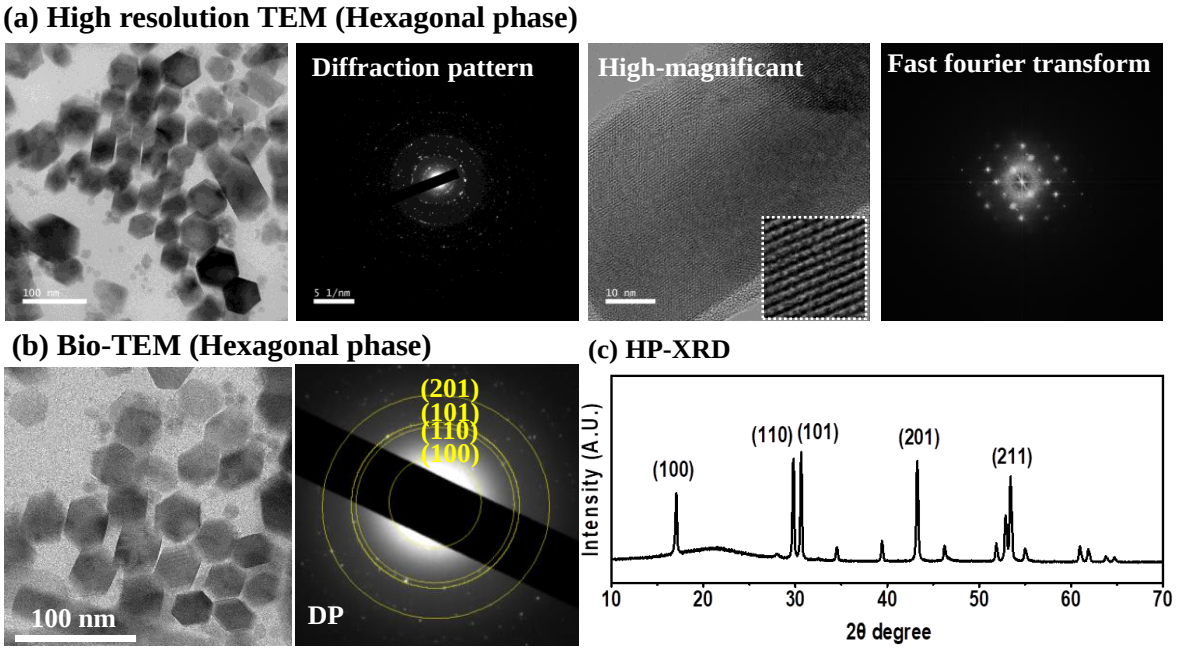

Figure 23. Comparison of the structure and morphology transition of UCNs embedded microstructures depending on sintering temperature.

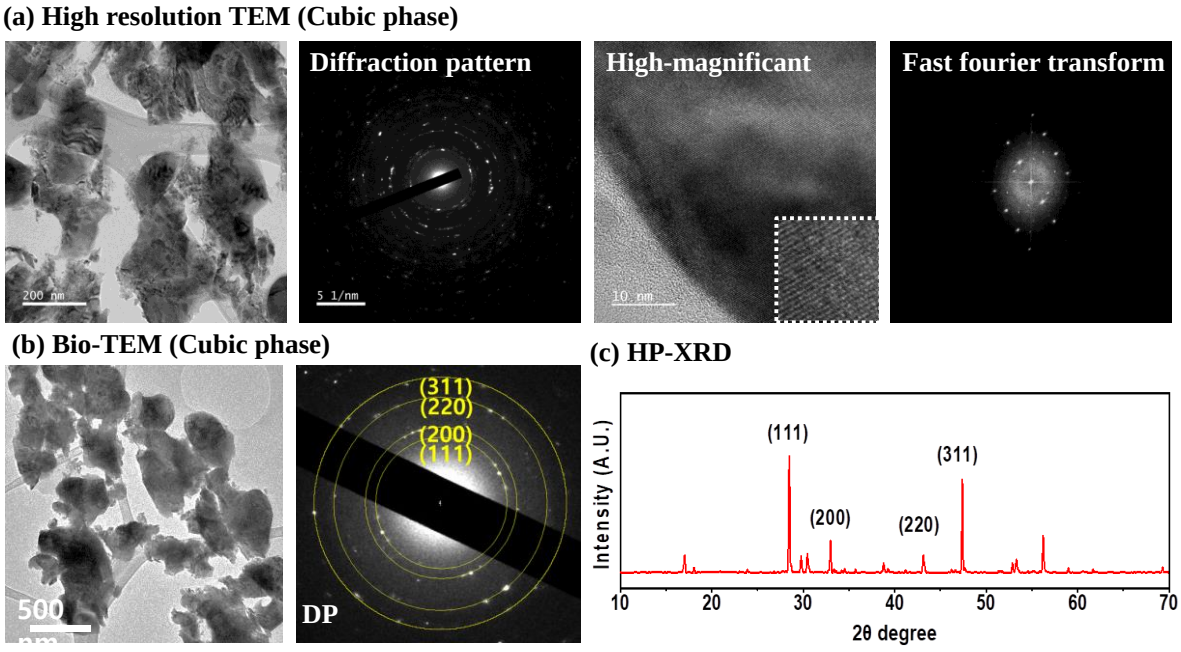

Figure 24. Comparison of the structure and morphology transition of UCNs embedded microstructures depending on sintering temperature.

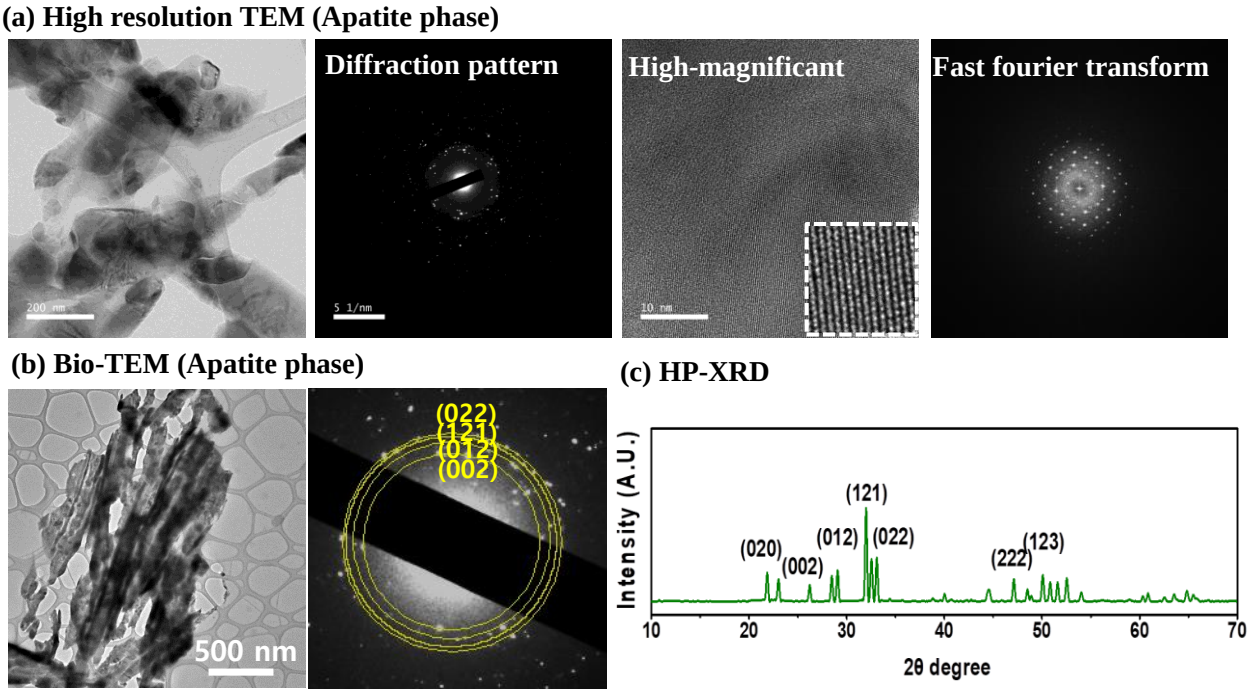

Figure 25. Comparison of the structure and morphology transition of UCNs embedded microstructures

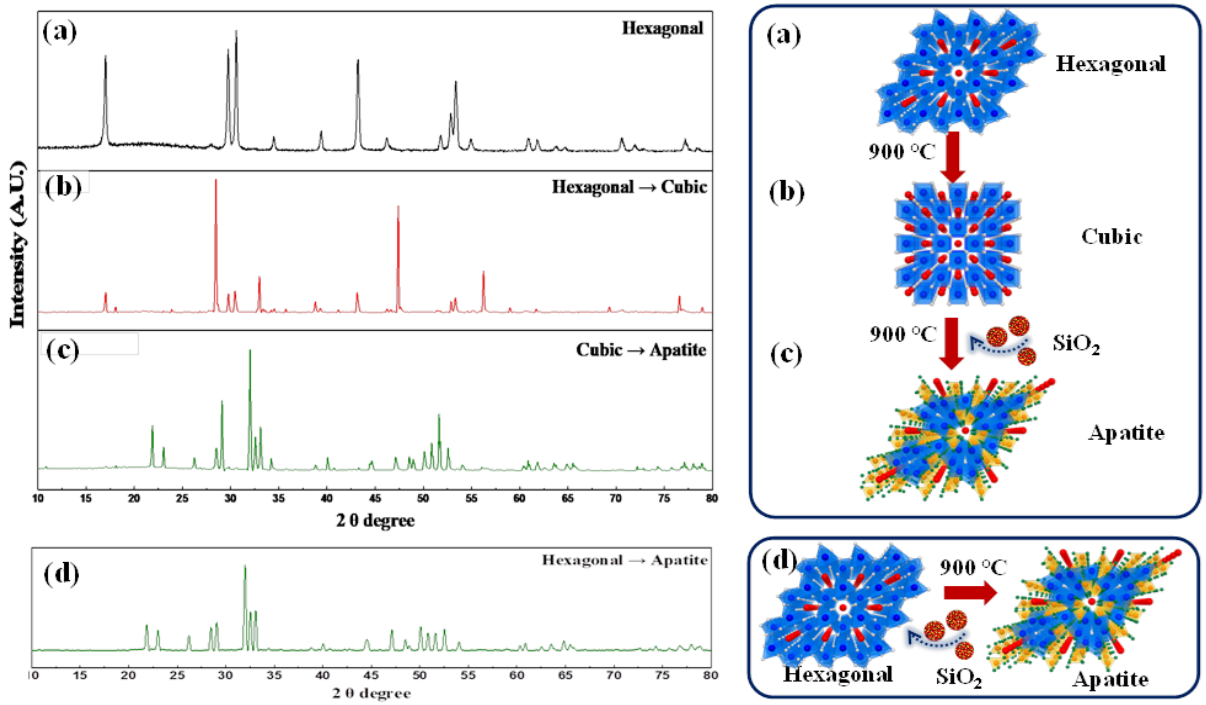

Figure 26. Multi-step annealing process (a) Pristine hexagonal XRD (b) Cubic phase of $NaGdF_4$ after annealing process without SiO_2 nanoparticles (c) Further annealing using adding to silica nanoparticles onto cubic phase (d) Direct phase transition from hexagonal to apatite with SiO_2

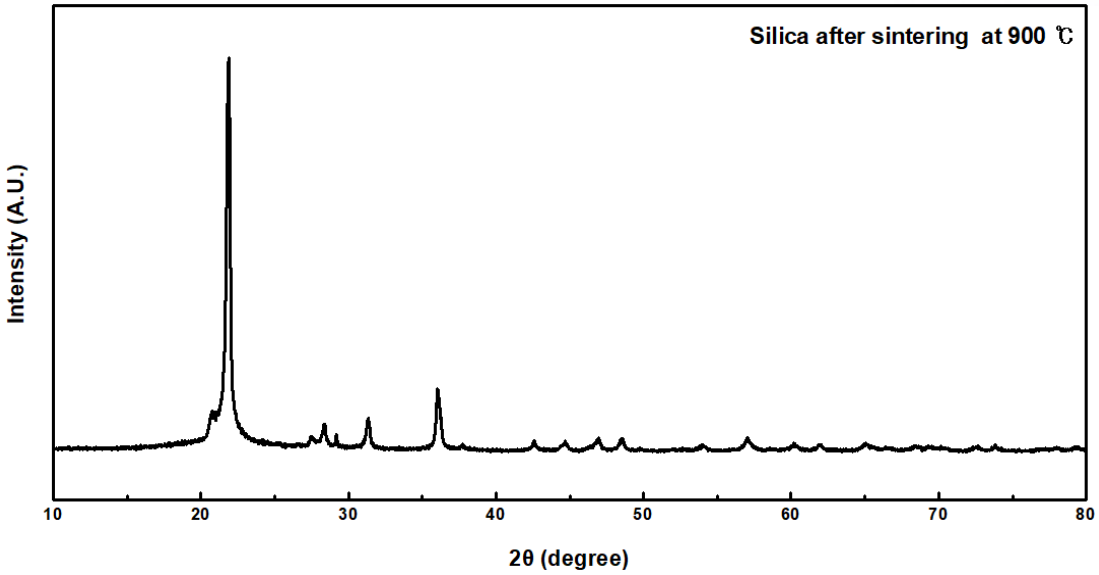

Figure 27. Comparision of XRD pattern of SiO_2 nanoparticles before and after sintering at 900 ℃

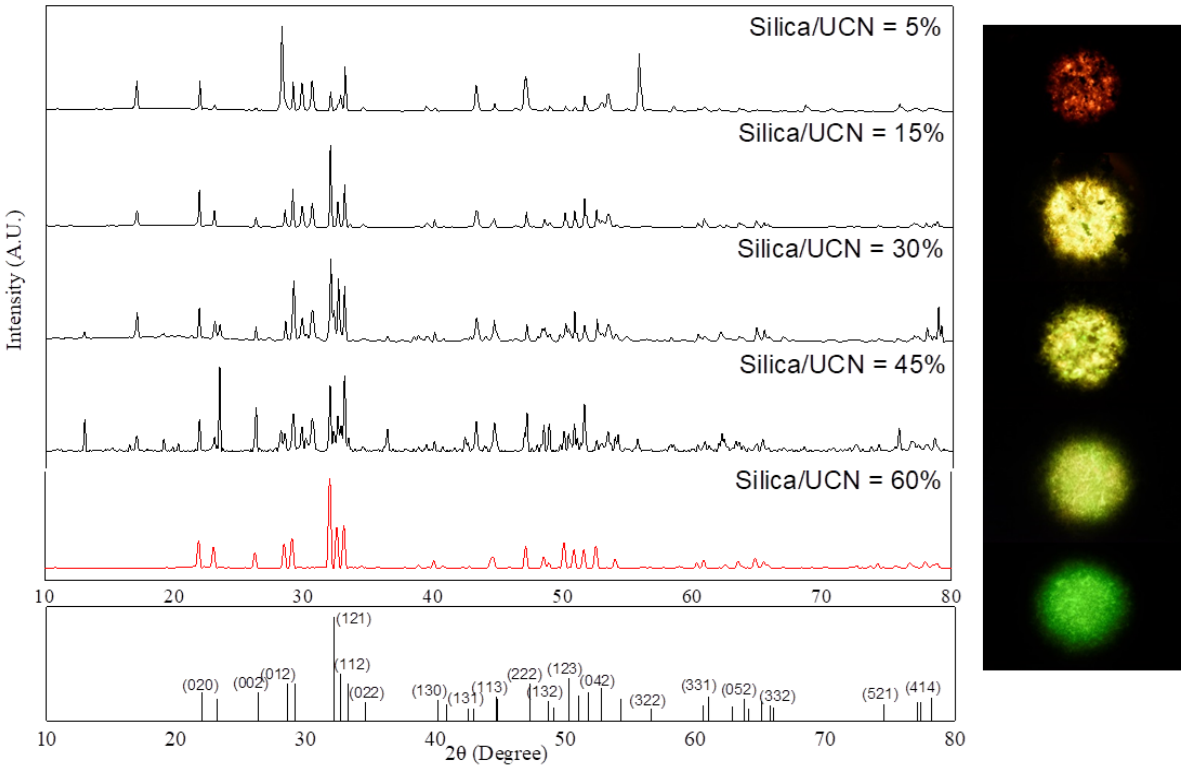

Figure 28. XRD pattern of UCNs depending on the concentration of SiO_2 nanoparticles ranged 5% to 60% (w/w ratio of SiO_2 nanoparticles and UCNs) after sintering at 900 ℃

3.6 UCNs embedded microstructures synthesis using a stop-flow lithography

We synthesized a microstructure with various forms of UCNs/SiO_2 nanoparticles interspersed using maskless photo-patterning with PDMS microfluidic channel. Oleic acid capped UCNs are easily dispersed in PUA/photo-initiator (PI)/SiO_2 nanoparticles. We inhibited leaching of UCNs and SiO_2 nanoparticles using photocurable PUA resin and synthesized microstructure using a stop-flow lithography technology. Stop-flow lithography (SFL) polymerizes microstructures via patterned ultraviolet radiation (365 nm) when the flow of photo-curable resin with UCNs dispersed stops, and then the resin flows normally again. It is a microstructure synthesis technology within PDMS microfluidic channels (Dendukuri et al., Lab Chip, 2007, 7, 818-828). When the flow of the resin in which the UCNs and the SiO_2 nanoparticles are dispersed stops, the microstructure are synthesized immediately via the photopolymerization process. Photopolymerization is a free radical reaction of photoinitiators decomposed by ultraviolet radiation and it is possible to synthesize microstructures with high throughput within a short period of time through repetitive synthetic processes inside the PDMS channel. We also freely manipulated the photomask using a digital micromirror device (DMD) containing micromirrors tilted by induced electrical signals (**Figure 29**). The DMD was able to mount the photomask by controlling the angle and direction of the micromirror. With this SFL technology, we synthesized striped particles using multiple laminar flows in the PDMS microfluidic channel (**Figure 29c**). In addition, this multiple laminar flows can be used to control the presence and location of SiO_2 nanoparticles to microstructures, and multi-color emissive microstructures can also be realized.

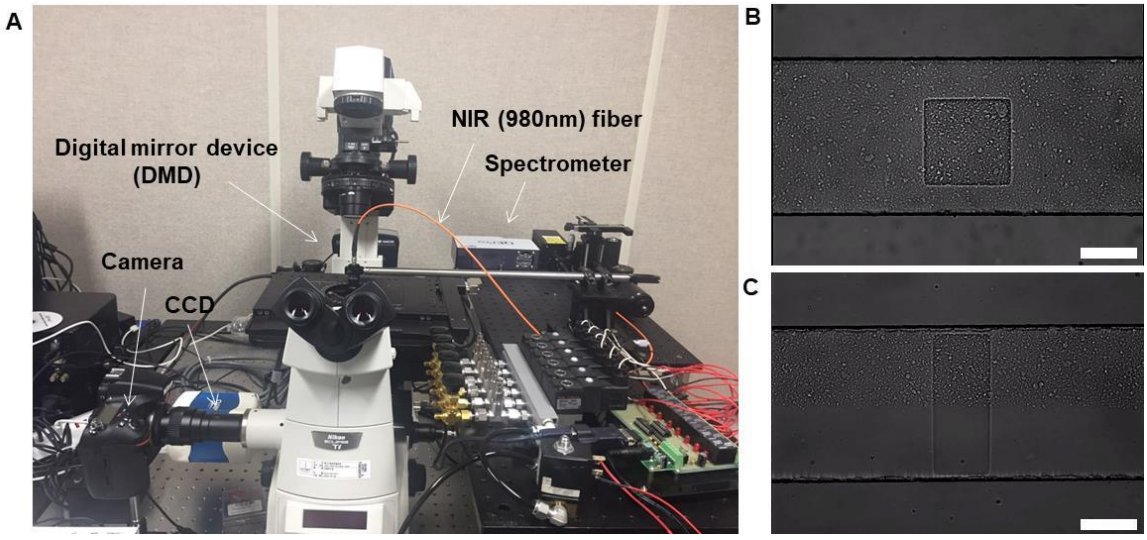

Figure 29. Stop-flow lithography setup to synthesize UCNs embedded microstructures (a) Optical image of SFL incorporated microscope (b) Optical image of UCNs and SiO_2 embedded microstructure in micropfluidic channel (c) with two-laminar flow

3.7 Application of UCNs embedded structures for multi-level security system

In order to demonstrate the utility of our system, we used maskless photo-patterning of PDMS microfluidic channels (Lee et al., Nat Mater 13 (5), 524-529) and the color change of microstructures containing UCNs of four colors (yellow, green, blue, white) was investigated (**Figure 30**). As a result, in the absence of SiO_2 nanoparticles, green and yellow turn to red, blue and white turn to blue. The changed red and blue had weak luminescent properties and it was difficult to distinguish between the naked eye with NIR (980 nm) laser source. However, on adding SiO_2 nanoparticles to UCNs, green and yellow are changed to bright green emission and blue and white are changed to bright blue. Therefore, we discovered that SiO_2 nanoparticles play an important role in achieving a bright luminescent color after annealing. It was also found that the tendency of change in color depending on the types of dopants. Er^{3+} doped UCNs (green, yellow) changed to red or green, but Tm^{3+} doped UCN (blue, white) changed to blue. Thus, it is possible to manipulate the annealing color by selecting the dopant atoms.

We performed spectral encoding of microstructures containing yellow (Y), green (G), white (W), blue (B) UCNs and SiO_2 nanoparticles (S). First, a double coded UCN microstructure constructed using two colors (Y, G) and SiO_2 nanoparticles shows three conversion procedures single to double, double to single, and double to double. Six encodings produced from two colors can show the differences in luminescence intensity, color and stripe after heat treatment (**Figure 31**).

SiO_2 assisted double-to-double and double-to-single color variations are also shown from binary architecture during the sintering process. The sectioned binary structure (yellow/blue) has changed to double color (green/blue) after sintering. Conversely, single color (Blue) was also obtained after sintering process from double colors (blue and White). These results proved the capability of multiple color and structure demonstration on encoding system (**Figure 31b**).

To expand the capacity of multi-color realization, the color additive method is developed (**Figure 32**). The achieved multi-color systems are the results of controlling the concentration of SiO_2 nanoparticles, color-mixing ratio, and types of UCNs color. Since the two kinds of colors were mixed, the spectrum result shows three emission peaks at wavelengths of 470 nm (blue), 550 nm (green) and 660 nm (red), and as the concentration of SiO_2 nanoparticles and the mixing ratio, the spectrum pattern was adjusted variously (**Figure 34**). However, in the absence of SiO_2 nanoparticles, the emission intensity of the resulting color is almost invisibly low (**Figure 34, 1~3**). However, when SiO_2 nanoparticles are added, the emission intensity increases according to the concentration of the SiO_2 nanoparticles, and various colors are obtained. This multicolor realization can be further expanded by controlling the mixing ratio of UCNs colors. With this development, we were able to control total 12 transition colors. Without SiO_2 nanoparticle on UCNs (**1~3**), the annealing color

emission is very weak under the NIR light source, and most of them are reddish emission. Even in the spectral data, the peaks of green (550 nm) and blue (470 nm) after the heat treatment sharply decrease, showing weak red light emission. However, when SiO_2 nanoparticles were added to UCNs, the emission intensity was bright according to the concentration of SiO_2 nanoparticles, the color mixing ratio and the types of colors, thus, the multi-color transition could be realized.

Finally, we developed synthesis system to create a multifunctional covert architecture containing hidden effects (**Figure 33**). This system is designed to produce a secretary structure by controlling the position of the stage and fabricating the microarray. Details are described in the experimental part 2.4. This technique realizes that hidden colors (green and red) appear after the thermal process. A simple yellow micro-post, when sintered at 300 ℃, the edge boundary has shown, and finally, at 900 ℃, it is possible to distinguish between green (inside) and red (outside) of a confidential structure. Utilizing these functions, we were able to realize the spectral covert features for anti-counterfeiting technology.

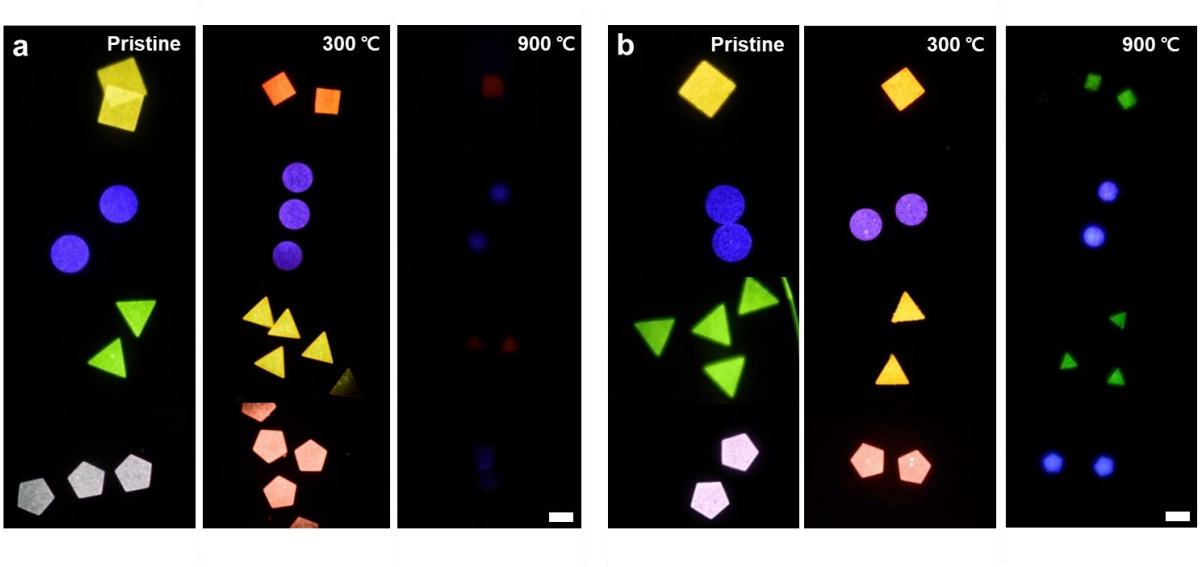

Figure 30. Synthesized diverse color and shape of UCNs embedded structures using a Stop-flow lithography (a) UCNs embedded structures without SiO_2 nanoparticles (b) SiO_2 integrated UCNs embedded structures before and after sintering 300 and 900 ℃

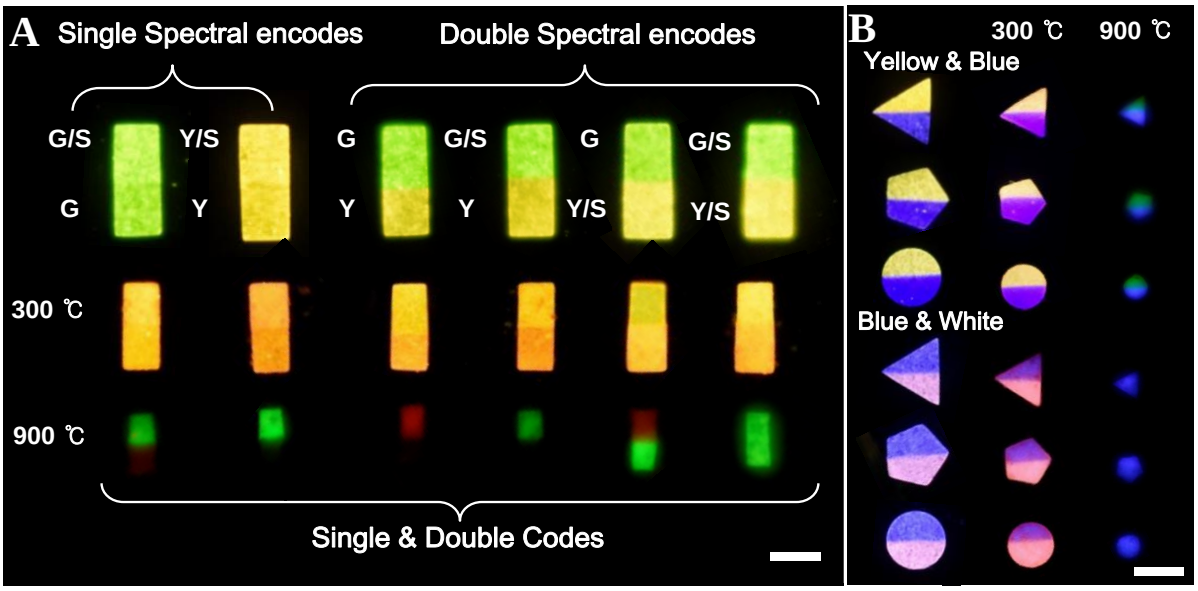

Figure 31. Applications of UCNs embedded microstructure for multi-level security system (a) Schematic diagram of stop-flow lithography (b) Single and double encode UCNs embedded microstructure using two-colors of UCNs

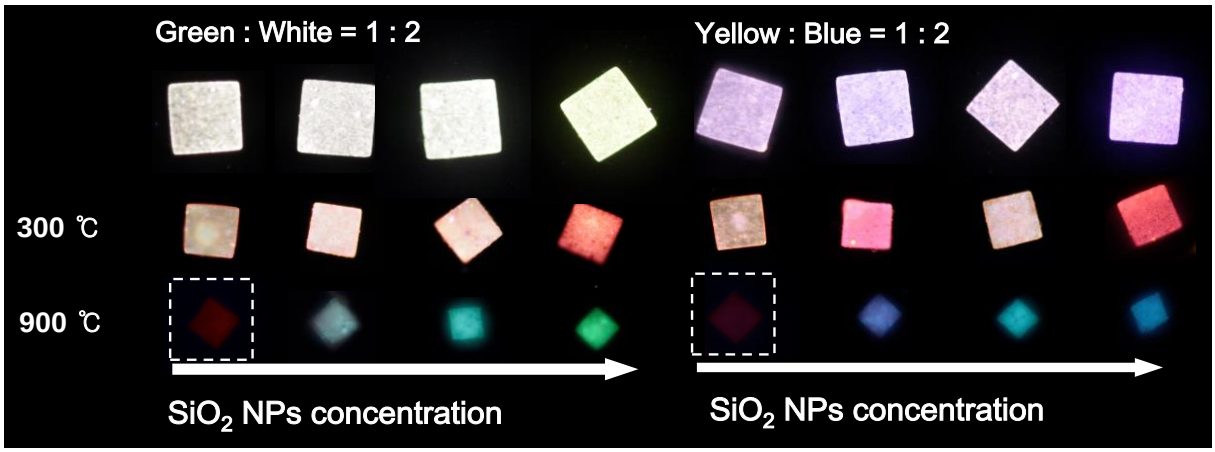

Figure 32. Mixing color UCNs embedded microstructure with different mixing ratio, color, and SiO_2 concentration

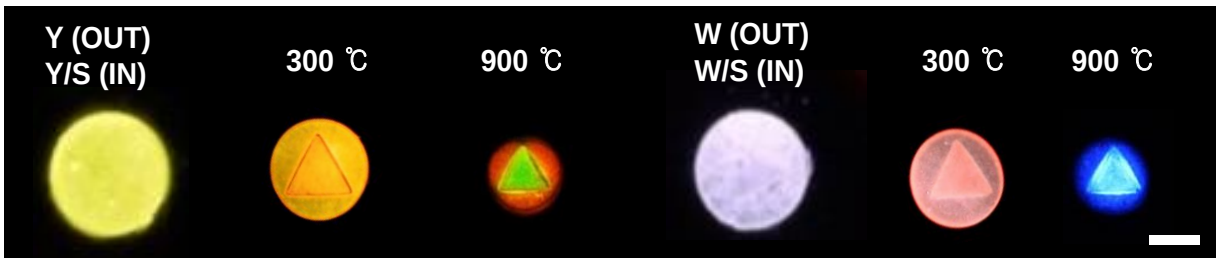

Figure 33. UCNs embedded covert microstructure with hidden effect after sintering process

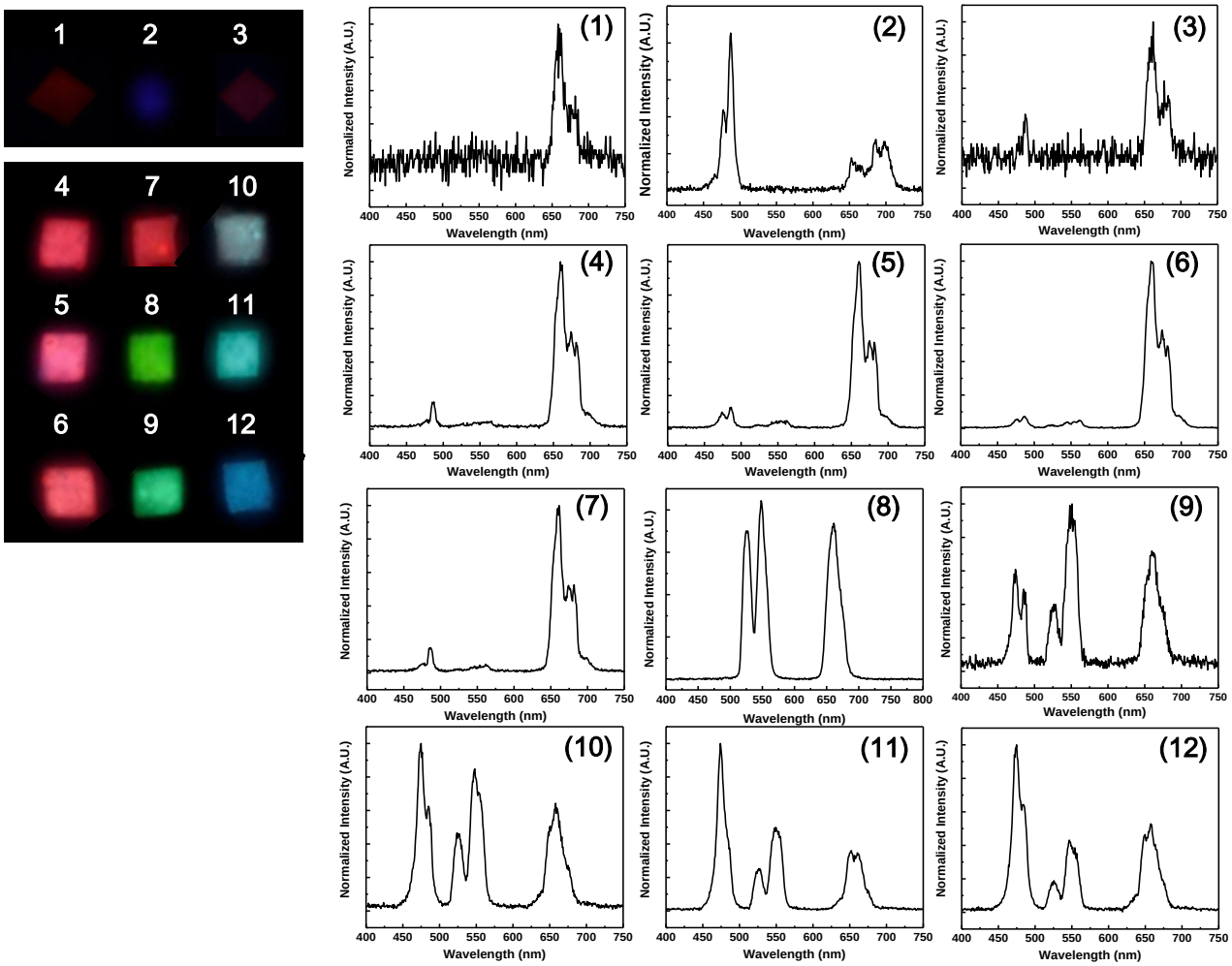

Figure 34. Multi-color realization and UC emission spectrum (1) ~ (3) Sintered color realization without SiO_2 nanoparticles. (4)~(12) Sintered color realization depending on the concentration of SiO_2 nanoparticles and UCN color blending ratio.

.

IV. CONCLUSION

In summary, we developed a novel luminescent color and phase transition technology of UCNs on inter-atomic scale. Originally, the emission color of UCNs is known to depend on the distance between lanthanide dopant ions. Therefore, in order to control the distance between dopant atoms, we use silica nanoparticles capable of sintering process at high temperature, silica nanoparticles dissolve in the host of UCNs during the annealing process and the distance of Er^{3+} dopants can be controlled. These results were investigated by SEM, TEM, XRD and FT-IR spectroscopy, and it was possible to confirm the color (yellow to green) and the phase transition (hexagonal to apatite) by the silica nanoparticles. Even after the thermal treatment, high crystallinity of annealed UCNs could be confirmed by the lattice fringe pattern confirmed by TEM analysis, and the phase transition was clearly demonstrated using XRD analysis. In addition, it was possible to obtain a multi-step phase transition (hexagonal-cubic-apatite) while progressing the multi-step annealing process, and this result shows that the SiO_2 nanoparticles is a phase former to apatite structure from any phase of UCNs with annealing process. Furthermore, in order to understand the phase and color transition of UCNs, the distance between Er^{3+} dopant atoms was compared by DFT calculation. As shown in the proposed energy diagram, we found that the emission color of UCNs is the influence of cross-relaxation process due to change in distance on inter-atomic scale.

We have also found that even the increase of luminescence intensity of SiO_2 nanoparticles assistence phase transition (hexagonal to apatite) as compared to the case of non-containing SiO_2 nanoparticles with phase transition (hexagonal to cubic) with color transition (yellow to red). As a result, apatite UCNs showed luminescence intensity about 2 orders of magnitude higher than the cubic structure due to high photon energy absorption rate irradiated by simulation calculation. On the whole, however, only three color transitions (red, blue, and green) could be acquired by color change during the annealing treatment. In order to solve such a short range of color tuning, a new method of color additive was developed. In order to expand the transition color range, we controlled silica nanoparticles concentration and mixed ratio of UCNs colors. Through this development we were able to prove multi-color adjustment after the annealing process. We also developed striped encoding microparticles and shape coded microparticles.

Finally, we created a covert structure involved hidden colors (green, red) after the annealing process. The synthesized confidential structure (yellow post) was transformed into a patterned structure containing secret colors. For these developments, we were able to adjust the multicolor transition with unique microparticles and realize the spectrum coordination for anti-counterfeiting technology.

V. REFERENCE

1. Chen, D., et al. (2016). "Ce^{3+} dopants-induced spectral conversion from green to red in the Yb/Ho: NaLuF4 self-crystallized nano-glass-ceramics." Journal of Alloys and Compounds 654: 151-156.

2. Dendukuri, D., et al. (2007). "Stop-flow lithography in a microfluidic device." Lab Chip 7(7): 818-828.

3. Ding, M., et al. (2013). "Molten salt synthesis of tetragonal LiYF4:Yb^{3+}/Ln^{3+} (Ln = Er, Tm, Ho) microcrystals with multicolor upconversion luminescence." CrystEngComm 15(30): 6015.

4. Dou, Q. and Y. Zhang (2011). "Tuning of the structure and emission spectra of upconversion nanocrystals by alkali ion doping." Langmuir 27(21): 13236-13241.

5. Idris, N. M., et al. (2012). "In vivo photodynamic therapy using upconversion nanoparticles as remote-controlled nanotransducers." Nat Med 18(10): 1580-1585.

6. Lee, J., et al. (2014). "Universal process-inert encoding architecture for polymer microparticles." Nat Mater 13(5): 524-529.

7. Lei, P., et al. (2017). "Ultrafast Synthesis of Novel Hexagonal Phase NaBiF4 Upconversion nanoparticles at Room Temperature." Adv Mater 29(22).

8. Li, Z., et al. (2011). "Modification of $NaYF_4$:Yb,Er@SiO_2 nanoparticles with Gold Nanocrystals for Tunable Green-to-Red Upconversion Emissions." The Journal of Physical Chemistry C 115(8): 3291-3296.

9. Li, Z. and Y. Zhang (2008). "An efficient and user-friendly method for the synthesis of hexagonal-phase $NaYF_4$:Yb, Er/Tm nanocrystals with controllable shape and upconversion fluorescence." Nanotechnology 19(34): 345606.

10. Liu, Q., et al. (2011). "Sub-10 nm hexagonal lanthanide-doped $NaLuF_4$ upconversion nanocrystals for sensitive bioimaging in vivo." J Am Chem Soc 133(43): 17122-17125.

11. Meruga, J. M., et al. (2014). "Red-green-blue printing using luminescence-upconversion inks." Journal of Materials Chemistry C 2(12): 2221.

12. Niu, W., et al. (2010). "A facile and general approach for the multicolor tuning of lanthanide-ion doped $NaYF_4$ upconversion nanoparticles within a fixed composition." Journal of Materials Chemistry 20(41): 9113.

13. Shepherd, R. F., et al. (2008). "Stop-Flow Lithography of Colloidal, Glass, and Silicon Microcomponents." Advanced Materials 20(24): 4734-4739.

14. Tian, G., et al. (2012). "Mn^{2+} dopant-controlled synthesis of $NaYF_4$:Yb/Er upconversion nanoparticles for in vivo imaging and drug delivery." Adv Mater 24(9): 1226-1231.

15. Wang, F., et al. (2010). "Simultaneous phase and size control of upconversion nanocrystals through lanthanide doping." Nature 463(7284): 1061-1065.

16. Wang, M., et al. (2011). "Upconversion nanoparticles: synthesis, surface modification and biological applications." Nanomedicine 7(6): 710-729.

17. Wang, M., et al. (2015). "NIR-induced highly sensitive detection of latent finger-marks by $NaYF_4$:Yb,Er upconversion nanoparticles in a dry powder state." Nano Res 8(6): 1800-1810.

18. You, M., et al. (2015). "Inkjet printing of upconversion nanoparticles for anti-counterfeit applications." Nanoscale 7(10): 4423-4431.

19. Zhang, L., et al. (2017). "The colour tuning of upconversion emission from green to red in $NaScF_4$:Yb^{3+}/Er^{3+} nanocrystals by adjusting the reaction time." Journal of Alloys and Compounds 699: 1-6.

20. Zhou, B., et al. (2015). "Controlling upconversion nanocrystals for emerging applications." Nat Nanotechnol 10(11): 924-936.

ACKNOWLEDGEMENTS

석사 과정 동안 항상 믿음으로 이끌어주시고 가르쳐주셨던 교수님께 가장 먼저 감사의 마음을 전하고 싶습니다. 항상 모든 학생을 한 명 씩 세심하게 조언해주시고 믿음을 주시는 교수님 덕분에 석사 생활 동안 많은 것을 배울 수 있었습니다. 교수님께 받은 가르침, 절대 잊지 않고 앞으로 더 발전하고 성숙한 제자가 되도록 하겠습니다.

그리고 공동연구를 진행하면서 많은 조언을 해주시고 학위 심사까지 맡아주신 곽상규 교수님과 강석주 교수님께도 감사의 말씀 전하고 싶습니다. 교수님 두 분께서 말씀해주셨던 세심한 조언들 덕분에 무사히 학위 심사와 논문까지 마무리할 수 있었습니다.

또한, 함께 연구를 이끌어나가면서 많은 것을 배울 수 있게 도와주셨던 이태경, 주세훈, 이주란, 박재현 박사님께도 감사드립니다. 연구를 함께 진행하면서 부족한 점이 많았는데 항상 이해해주시고 가르쳐주셔서 정말 감사합니다.

석사과정을 진행하면서 2년 동안 가장 많이 의지하고 동고동락하였던 우리 연구실 석사, 박사님들, 항상 가족 같은 분위기에서 연구를 함께 토의하고 진행해나갈 수 있어서 정말 행복했습니다. 앞으로도 우리 연구실 승승장구하여 각자의 꿈을 모두 이루시기를 간절히 바라며 항상 응원하겠습니다. 그동안 너무 감사했습니다.

마지막으로 사랑하는 우리 가족들, 지금까지 받은 과분한 사랑을 앞으로 차근히 보답할게요. 항상 응원해주시고 믿고 기다려주셔서 정말 감사합니다. 앞으로 더 든든한 딸이 될게요. 사랑합니다.